Application Performance of Unmanned Aerial Systems (UAS) for Seeding Cover Crop

by

Jacob Earl Sizemore

A thesis submitted to the Graduate Faculty of
Auburn University
in partial fulfillment of the
requirements for the Degree of
Master of Science

Auburn, Alabama
May 2nd, 2026

Keywords : Cover Crop, UAS, Spreading, Distribution Uniformity

Copyright 2026 by Jacob Earl Sizemore

Approved by

Dr. Simerjeet Virk, Chair, Associate Professor, Department of Biosystems Engineering
Dr. Steve Li, Associate Professor, Department of Crop, Soils & Environmental Sciences
Dr. Audrey Gamble, Associate Professor, Department of Crop, Soils & Environmental Sciences
Dr. John Linhoss, Assistant Professor, Department of Biosystems Engineering

Abstract

The use of unmanned aerial systems (UAS) for applying dry solid products, especially cover crop seed, has increased rapidly in the United States in recent years. Limited information currently exists on the application performance of dry spreading systems on UAS; therefore, studies were conducted to evaluate the spreading performance, in terms of applied rate and distribution uniformity, of cereal rye – one of the widely used cover crops – applied with a commercially available UAS (DJI Agras T25). The first study evaluated the calibration and metering accuracy of the UAS, while also investigating the material distribution within the single-pass and simulated overlap patterns across varying application rates (22.4, 33.6, 44.8, 56.0 & 64.3 kg ha^{-1}) and flight speeds (6, 7, 8, 9 & 10 m s^{-1}). Results showed that the actual flow rate (kg min^{-1}) differed from the flow rates suggested by the manufacturer's internal calibration, resulting in significant under-application of cereal rye (9.5% – 17.7%) during the field tests. The single-pass spread patterns showed leftward skewness, indicating greater material distribution (51% to 64%) towards the left and lower material deposition (29% to 40%) towards the right of the spread swath. The simulated overlap spread pattern analysis indicated no effect of application rate or flight speed on the distribution uniformity of cereal rye; however, application method affected spreading uniformity, with the one-direction application method (CV = 19 – 28 %) exhibiting improved material deposition within the swath compared to the progressive method (CV = 22 – 39 %). The second study investigated the effects of application height (3.0, 3.8, and 4.6 m) and spinner-disc speed (700, 1000, and 1300 rpm) on the distribution uniformity of cereal rye within the swath

applied with the UAS. Additionally, the effects of hopper metering gate design (medium and large gates with varied-size openings) and spinner-disc design (straight and curved vanes) on material distribution were evaluated across varying application rates. Results showed that both application height and spinner-disc speed affected cereal rye distribution within the swath, with single-pass spread patterns showing lower material deposition at an application height of 4.6 m and a spinner-disc speed of 700 rpm compared to other heights and speeds. Similarly, the maximum single-pass swath increased with application height (from 11.0 to 13.4 m) and spinner-disc speed (from 10.2 to 14.5 m). The distribution uniformity for overlap patterns was similar across application heights (CV = 30 – 33 %), whereas the spinner-disc speeds of 1000 and 1300 rpm (CV values of 31 and 26, respectively) demonstrated improved spreading uniformity compared to the 700 rpm (CV = 38%). The medium metering gate showed a wider single-pass swath than the large gate, but the mean applied rate and distribution uniformity (CV = 37%) were similar across the two gate designs. Similarly, the spinner-disc with curved vanes exhibited greater material deposition, a wider single-pass swath, and greater leftward skewness than the straight-vane disc; however, the spreading distribution for the overlap spread pattern was comparable (CV = 29 – 34 %) across both disc designs. Overall, the results from these studies show promising potential for UAS as an effective technology for applying cover crop seed; however, proper calibration and the selection of optimal operational parameters are highly recommended to ensure accurate and uniform application.

Artificial Intelligence (AI) Use Disclosure Statement

In the preparation of this thesis, the following Artificial Intelligence (AI) tools were used: Microsoft Copilot & Canva Magic Studio. These tools were primarily used to remove backgrounds from images or to produce translucent backgrounds in some images. The images were used for figures within this thesis to more clearly present design characteristics highlighted in the surrounding text. The author acknowledges full responsibility for the intellectual content of this work and has ensured that all AI-assisted sections have been reviewed and revised for accuracy and appropriate academic style. All AI-generated content was reviewed and validated for relevance, appropriateness, and accuracy before incorporation into the final document to maintain the scholarly integrity of this research.

Digital Accessibility Use Disclosure Statement

In the preparation of this thesis / dissertation, the following digital accessibility tools were used to ensure this document complies with federal requirements: Microsoft Word. The author acknowledges full responsibility for the intellectual content of this work and has made a good faith effort to comply with digital accessibility requirements in publishing, wherein the nature of the content does not significantly change in order to do so. Furthermore, all content has been reviewed and revised to meet these requirements prior to final publication.

Acknowledgments

First and foremost, I would like to thank my wife, Caroline, for the much-needed support and encouragement during my time in Graduate School. From assisting me in weighing samples to hearing my keyboard click furiously late into the night, she deserves much credit for her support and patience. I would also like to thank my close friends and family for their encouragement. Their interjections of humor and grace provided lighthearted moments that kept me from "burning out". I would begin to list each of you, but I would surely miss someone important. As such, those that I am referring to will know who you are.

To my teammates and friends, Dalton Beasley, Shubhdeep Singh, and Louis Harris, thank you for the help you provided during long field days collecting data for this project, as well as for the various preparation tasks needed for those days. I can only hope that I have repaid each of you for the immense amount of help you provided.

To my major professor, Dr. Simerjeet Virk, thank you for allowing me to join your team when you arrived in Auburn. I have truly enjoyed working under your guidance and have gained an immense amount of knowledge relating to technology in agriculture. Thank you for allowing me to also take part in the rebirth of precision agriculture here at Auburn, a truly needed venture that will benefit producers across the state. To my committee members, Drs. Steve Li, Audrey Gamble, and John Linhoss, thank you for the guidance before and during my project. Each of you provided insight and knowledge into a completely new subject to me. Your support and assistance will surely be reflected in the pages that follow.

Table of Contents

List of Tables

List of Figures

List of Abbreviations

AL CORS	Alabama Continuously Operating Reference Stations
ASABE	American Society of Agricultural and Biosystems Engineers
ASAE	American Society of Agricultural Engineers
CV	Coefficient of Variation
RTK	Real Time Kinematic
UAS	Unmanned Aerial Systems
US	United States
USDA	United States Department of Agriculture

Chapter One

Introduction

1.1 Introduction

Today, producers are more productive, efficient, and environmentally responsible than ever before due to technological advancements over the past century. These advancements range from innovations in seed genetics to highly mechanized equipment on nearly all farms today. Over the last 40 years, another wave of agricultural advancement has occurred with the introduction of precision farming practices and the utilization of geospatial technologies for site-specific application of crop inputs. Júnior et al. (2024) describe precision agriculture as the use of advanced technologies, complex data analysis techniques, and cutting-edge tools to address temporal and spatial variability in agricultural systems. The International Society of Precision Agriculture (2024) defines precision agriculture as a management strategy that uses gathered information to support management decisions to improve resource use, productivity, quality, profitability, and the sustainability of agricultural production. These precision agriculture systems range from planting and spraying technologies to variable-rate application and yield-monitoring systems on harvesters. These technologies have enabled producers to increase crop yields and productivity, offering a variety of technological solutions to improve efficiency and profitability on their farms.

With the evolution of technology in agriculture, Unmanned Aerial Systems (UAS, also commonly referred to as drones) have become an increasingly popular tool for producers around the world in recent years. While the use of UAS in agriculture in the United States has increased recently, they have been utilized in Asian agriculture for nearly 40 years, with the first UAS being released in the 1980s. According to Xiongkui (2017), Japan was the first country to develop and release a UAS platform in 1985 with the Yamaha R50, a gasoline-powered helicopter with a 5 kg

payload. Since then, technological innovations paramount to UAS design have enabled manufacturers to significantly increase payload capacity and field efficiency of newer platforms. These gains have further facilitated a rapid growth in UAS applications in Asia, with over 71.3 million hectares of agricultural land treated in 2021 in China alone (Ozkan, 2024). Though the United States has been slower to adopt UAS technologies than Asian countries, their usage in US agriculture has grown substantially in recent years, with over 4.1 million hectares treated in 2024 (American Spray Drone Coalition, 2024).

While UASs have primarily been used to apply agrochemicals (e.g., herbicides and fungicides) to agricultural crops, their use for applying dry solid materials, especially small seeds and fertilizer granules, has also increased rapidly. The rapid growth in UAS adoption can be attributed to the benefits that aerial applications provide over traditional ground-based methods, including reduced human exposure to pesticides during applications. Although effective, traditional methods of applying crop inputs can increase soil compaction over time due to the weight of machinery, negatively impacting cash crop yields (Shaheb et al., 2021). Whalley et al. (1994) also suggested a negative impact of soil compaction on crop root structure, which can not only lead to short-term yield loss but also to long-term soil regeneration and rainwater absorption issues. Soil and crop quality are also affected by equipment use under unfavorable field conditions, such as excessive moisture or crop height. Aerial applications with manned aircraft do alleviate some of the issues associated with ground equipment and have been utilized in agricultural production since the early 1920s (Kraus, 2021). However, manned aircraft applications pose their own set of challenges, including an increased risk of collision with trees or power lines due to low-altitude operations and weather restrictions (NTSB, 2014). While UAS applications provide similar benefits to manned aerial applications, they also offer additional advantages, such as precision applications near

sensitive areas or in uneven terrain that would not be ideal for manned aircraft (Teske et al., 2018). Furthermore, the small size and irregular shape of most agricultural fields, especially in the southeastern United States, make both ground and aerial application with manned aircraft highly inefficient. UAS can provide more efficient and effective applications in these fields through their inherent flight performance, as well as through flight planning software that allows users to configure flight operations to the field environment.

Given their advantages, the use of UAS to seed cover crops in the US is increasing rapidly. In agriculture, cover crops are well known for their numerous benefits, such as improved soil aggregate stability (Dapaah & Vyn, 1998), weed reduction (Sarrantonio & Gallandt, 2003), and carbon sequestration in the soil (Dabney et al., 2001). However, cover crop species can vary in physical properties, such as seed shape or density, and these properties affect flight ballistics of the seeds (Hofstee & Huisman, 1990; Teske et al., 2007). Given that UAS spreading performance has not been investigated to the extent that agrochemical applications have been, there is a lack of understanding of how these systems perform under various application conditions. Specifically, the interactions between dry material particles and various UAS spreading parameters, such as flight height, speed, and route overlap spacing (effective swath), are not well understood. In liquid applications, on-target spraying of pesticides is paramount to avoid drift and ensure the correct concentrations are applied to the intended target (Bird et al., 1996). There are similar concerns with the application of dry material, as inaccurate applications can lead to economic losses and often undesirable field results (Roth & Field, 1992). Therefore, it is important to understand their application performance in terms of metering accuracy and distribution uniformity so that UAS can be utilized for effective cover crop seeding and application of other dry materials.

1.2 Rationale

UAS adoption in agriculture in the United States has increased rapidly in recent years. Many new applications of UAS technology have become more common, including applying both liquid and dry materials. Liquid applications have been thoroughly investigated, with considerable implications for improving application quality relative to various UAS design features and the effectiveness of aerial application of agrochemicals. These include examining different nozzle types (hydraulic versus atomizers), comparing pesticide efficacy compared to traditional application methods, and the effect of various operational parameters such as flight height, speed, application rate, etc., on spray coverage and efficiency. However, limited research is currently available on the application of dry materials with UAS. Although few recent studies have examined the application of both fertilizer and cover crop seed with UAS, much remains unknown. Additionally, some previous research may no longer reflect the technologies currently available on UAS platforms. Given the growing interest, especially in cover crop seeding with UAS, there is a clear need to investigate how various operational parameters and system component designs of commercially available UAS platforms affect the application rate and distribution uniformity within the swath. Further investigation into these subjects and the dissemination of research findings will enable the establishment of best practices for effective utilization of these technologies.

1.3 Objectives

The overall goal of this research was to evaluate the application performance of dry spreading systems on UAS when applying a cover crop (cereal rye) seed. The specific objectives of this research were as follows:

1) Evaluate the metering accuracy of a dry spreading system on a commercially available UAS for the application of cover crop seed (cereal rye).
2) Investigate the spread distribution and uniformity of cereal rye applied with UAS at varying application rates and flight speeds.
3) Analyze the influence of application height and spinner-disc speed on the distribution uniformity of cover crop (cereal rye) seed applied with a UAS.
4) Examine the effect of metering gate and spinner-disc design on the spreading distribution of cover crop (cereal rye) seed applied with a UAS

1.4 Thesis Outline

This thesis is organized into five chapters. Chapter 1 introduces UAS as relevant to agriculture today, highlights the growing interest in applying dry materials with UAS, and provides a rationale for the research undertaken in this thesis. Chapter 2 provides information on UAS spreader components and outlines the different metering and spreading systems currently available on the latest models. This chapter also provides a brief review of the current literature on the use of dry spreader systems on UAS for dry material applications. Chapter 3 investigates the calibration and metering accuracy of a spreading system on a commercially available UAS for the application of cereal rye, while also determining the effect of application rate and flight speed on distribution uniformity within the swath. Chapter 4 examines the effects of various operational and structural parameters, including application height, spinner-disc speed and design, and metering gate design, on the distribution uniformity of cereal rye applied with a UAS. Chapter 5 briefly summarizes the research findings and provides conclusions and recommendations to guide future efforts on the use of UAS for spreading dry materials.

Chapter Two

Background & Literature Review

2.1 UAS Platforms & Components

Since the Yamaha R50 was introduced in 1985, UAS platforms have steadily increased in size and payload capacity. Currently, the largest commercially available UAS in the United States has a payload of up to 101 kg of dry material (Hylio AG-272, Hylio Inc., Richmond, Texas). Even smaller platforms, such as the DJI Agras T25 (SZ DJI Technology Co., Shenzhen, China), have a 25 kg payload, more than five times the R50's capacity. This greater capacity, coupled with increased battery endurance, allows operators to achieve a higher field efficiency, reducing the downtime and the number of refills. Unlike previous generations of UAS platforms, modern systems are now designed with interchangeable liquid and dry tanks to maximize the application capacity for both agrochemicals and dry granular products. These newer UAS platforms come with various options to easily interchange between the liquid solution tank and the dry material tank. Some manufacturers allow for the entire propulsion system to be detached and reattached to a new chassis, while others simply offer the option to swap the tank on the same chassis.

The first few sections of this chapter cover the various components and other information relevant to the application of dry materials using modern UAS platforms, while the latter section reviews the available research on the use of UAS for spreading dry materials and the effects of different application parameters on material distribution within the swath.

2.1.1 UAS Design, Components, & Software

While earlier UAS models had six to eight arms, each with an individual rotor, the latest UAS platforms use a four-arm layout with one or two motors per arm. This quadcopter arrangement is

typically powered by one or two large-capacity batteries, typically located near the center of the platform.

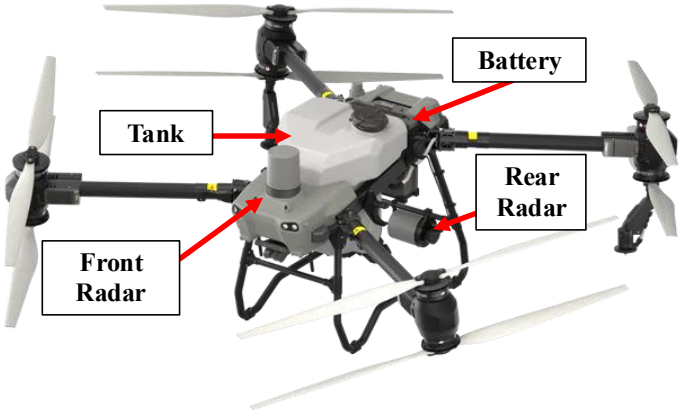

Figure 2.1. DJI Agras T50 with different components labeled: an interchangeable tank, forward obstacle avoidance radar, battery location, and rear obstacle avoidance radar.

Figure 2.1 depicts different components of a common UAS platform (DJI Agras T50). Although some manufacturers may design their platforms with slight alterations to the battery and radar locations, this general layout is very prevalent among most commercially available UASs. The interchangeable tank, and in some designs, an interchangeable chassis, are located at the center of the UAS frame. This central location for both the tank and battery allows for better weight distribution and flight performance. Most modern UAS platforms are also equipped with obstacle avoidance radars and sensors. These technologies enable the UAS to seamlessly integrate with proprietary software on controllers and/or smartphone applications to assist in creating flight plans and missions. To create a flight plan, an operator can designate an application area by adding points and areas on the controller using satellite imagery for spatial reference. This flight plan can then be executed in various ways. Most manufacturers have configured their software to enable autonomous flight, allowing the UAS to fly and conduct missions (applications) without human control. For example, XAG (manufacturer of the P100 and P150 UAS platforms) offers the XAG One app (XAG Co., Ltd, Guangzhou, China) for mission planning and flight parameter alterations,

such as flight height, application rate, and flight speed. During flight, application data and other flight information, such as flight speed and altitude, are also reported to the operator via the controller or the app. This data is useful for monitoring the UAS's in-flight performance and enabling the operator to make desired changes to the application parameters. The UAS software uses incoming data to adjust the product flow rate, keeping it closer to a target rate specified by the operator. Given the ability to fly autonomously, partially autonomously, and manually, users are offered a wide range of options within the flight planning software to apply products within the target area.

2.1.2 Metering Systems for Dry Materials

Among the UAS platforms currently available in the United States, there are two prominent spreader system designs for dry material applications. The first utilizes a single, horizontally mounted spreader disc that dispenses material across the swath. The manufacturers that utilize this design include DJI, EAVision (Suzhou Eavision Robotic Technologies Co., Ltd, Suzhou, China), and Hylio. These systems typically use a dry tank that relies on gravity to flow material through a metering gate onto the spinner disc mounted below [Figure 2.2(a)]. Manufacturers offer different metering (or feed) gate options with varying openings, allowing the operator to use the metering gate best suited to the type of material to be spread. Generally, granular products with smaller particle sizes require metering gates with smaller openings and vice versa. The newest models released by DJI and EA Vision at the time of writing use a horizontally mounted auger below the tank [Figure 2.2(b)] to meter material rather than a metering gate. Each manufacturer offers several options for auger screws with different flight (spiral-shaped helical blades coiled around a center shaft) spacing and sizes. This is intended to allow operators to select an auger based on the type of

material to be spread, with a large auger designed to handle large rates or large granular materials. Similarly, small augers are recommended for small materials or low flow rates.

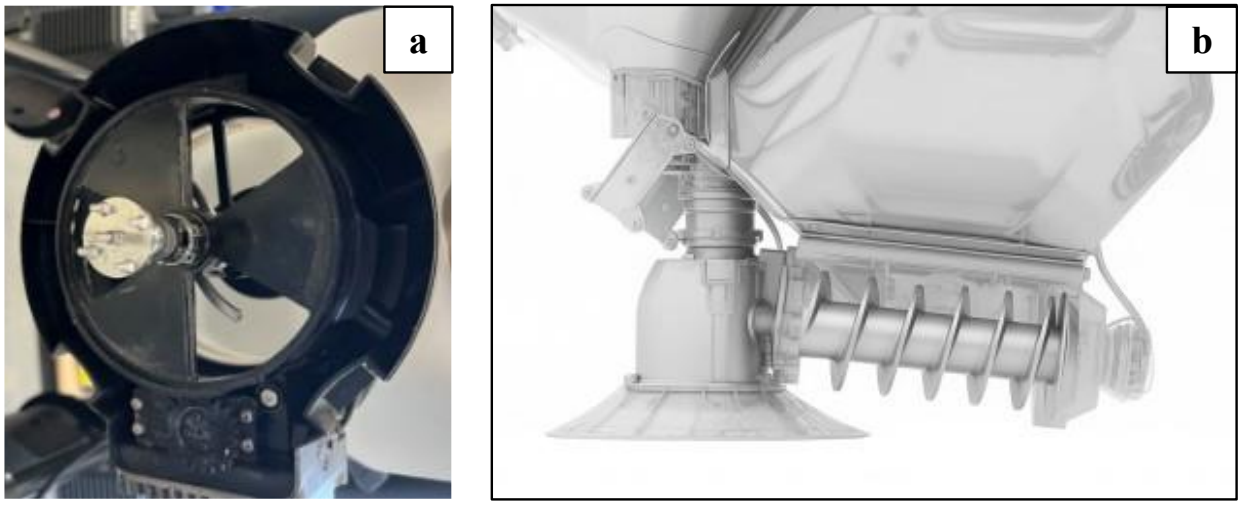

Figure 2.2. a) Illustration of a gravity-fed type metering gate on a DJI T25, and b) an auger type metering system on a DJI Agras T70.

2.1.3 Spreading Systems for Broadcasting Dry Materials

Once the material is metered from the hopper, there are two types of broadcast systems currently utilized by UAS manufacturers. The first design utilizes a single horizontal spinner-disc mounted below or behind the metering system's outlet. These discs are typically designed with straight, curved, or a combination of both vane types. The speed of these discs can be adjusted via the UAS controller, theoretically enabling more precise control of material distribution. Figure 2.3(a) depicts a common single-disc spreader, along with Figure 2.3(b & c) showcasing two spreading disc designs. On most systems, the spinner disc is covered by a shroud to help deflect material down into the swath. Manufacturers such as DJI, EAVision, and Hylio typically use this type of single-disc spreader system on their UAS platforms.

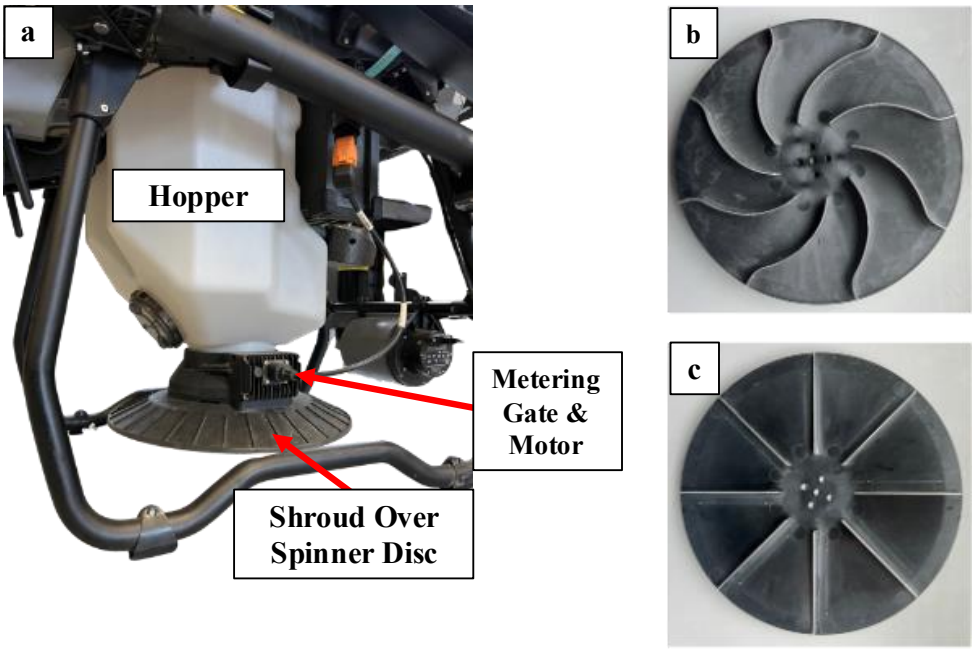

Figure 2.3. a) Illustration of a typical spinner disc system with different components labelled, b) Spinner disc with curved vanes, and c) Spinner disc with straight or flat vanes.

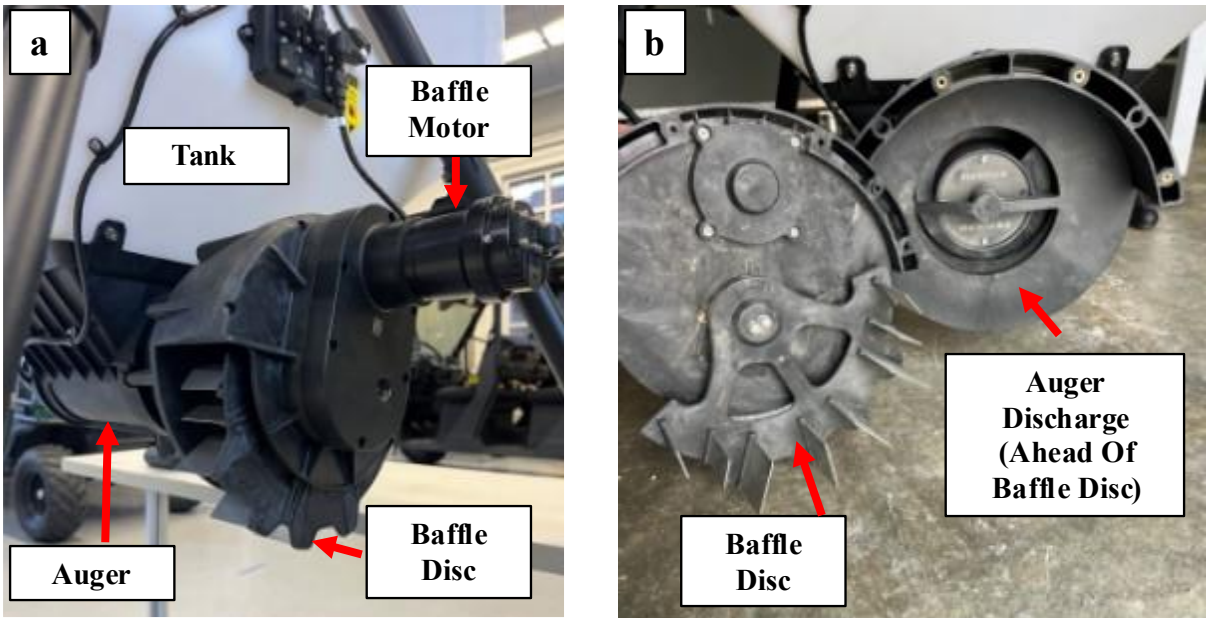

Figure 2.4. a) Vertically mounted disc with baffles on XAG P150 that rotates back and forth to spread material across the swath, and b) Baffle disc assembly displaying the auger discharge area.

The second type of spreading system design consists of one or two vertically mounted discs with baffles that oscillate left and right to distribute material across a swath; XAG is the most well-

known manufacturer that uses this design. The XAG UAS platform utilizes a horizontally mounted auger beneath the tank to deliver material to the discs, similar to the newest DJI and EAVision designs (Figure 2.4). These manufacturers also offer augers of varying sizes that can be installed beneath the tank, allowing users to easily interchange the correct auger size for the subject material.

2.1.4 UAS Spreader Calibration for Dry Materials

Regardless of the type of metering or spreading system, proper calibration of the UAS is important and recommended by all UAS manufacturers to apply the desired rate. Most manufacturers also provide an internal calibration process or steps to verify the applied rate. However, the exact process can differ slightly between different manufacturers. For example, DJI uses an internal procedure that requires the user to place their UAS between two raised objects, remove the spinner disc, and place a container beneath the gate, as illustrated in Figure 2.5(b). Once the hopper is approximately 80% full, the software prompts the user to select the metering gate currently installed in the system. The system will then automatically begin a calibration, with the resulting calibration then named and saved for future use [Figure 2.5 (a)]. The resultant calibration provides a graph depicting the increase in material flow as the metering gate's opening increases, with a maximum flow rate in pounds per minute at 100% metering gate opening. For newer generations of DJI Agras models that use an auger instead of a hopper gate, the procedure is the same, except that the installed auger size is selected rather than a metering gate.

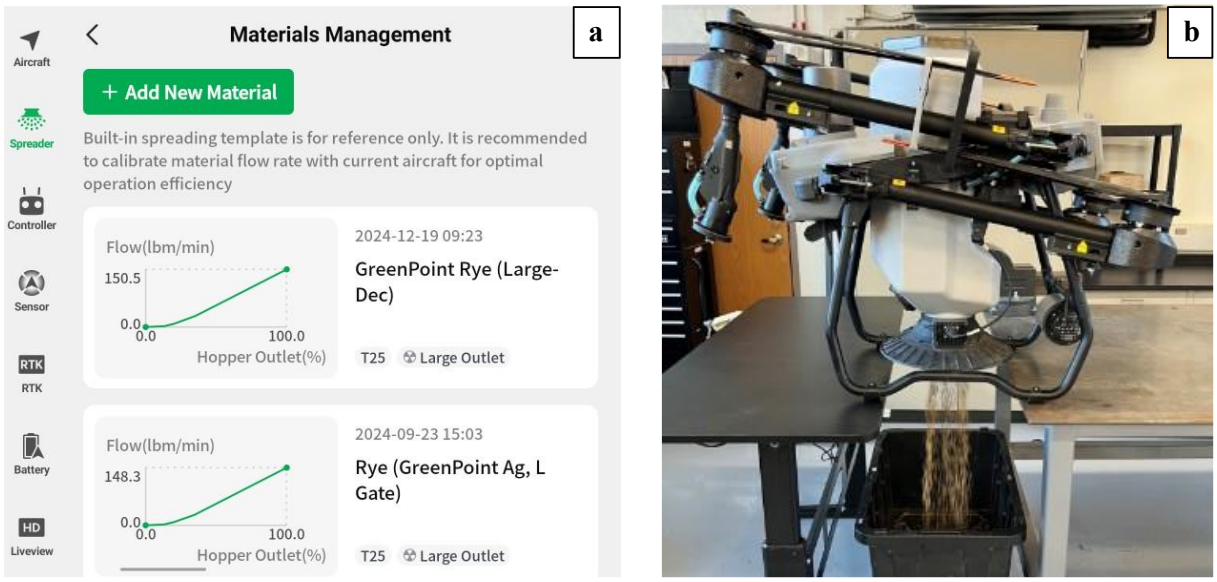

Figure 2.5. a) Materials management page on a DJI Agras controller and b) DJI Agras T25 propped between two raised objects undergoing a material calibration.

XAG uses a similar calibration procedure up to the selection of the metering gate (auger) in their models. Once the currently installed auger is selected, the system will begin a 20-second calibration, maintaining a constant auger speed throughout. Upon completion of the calibration, the dispensed material is weighed and entered into the controller to complete the material calibration process. No visual flow rate graph is provided, as in the DJI system.

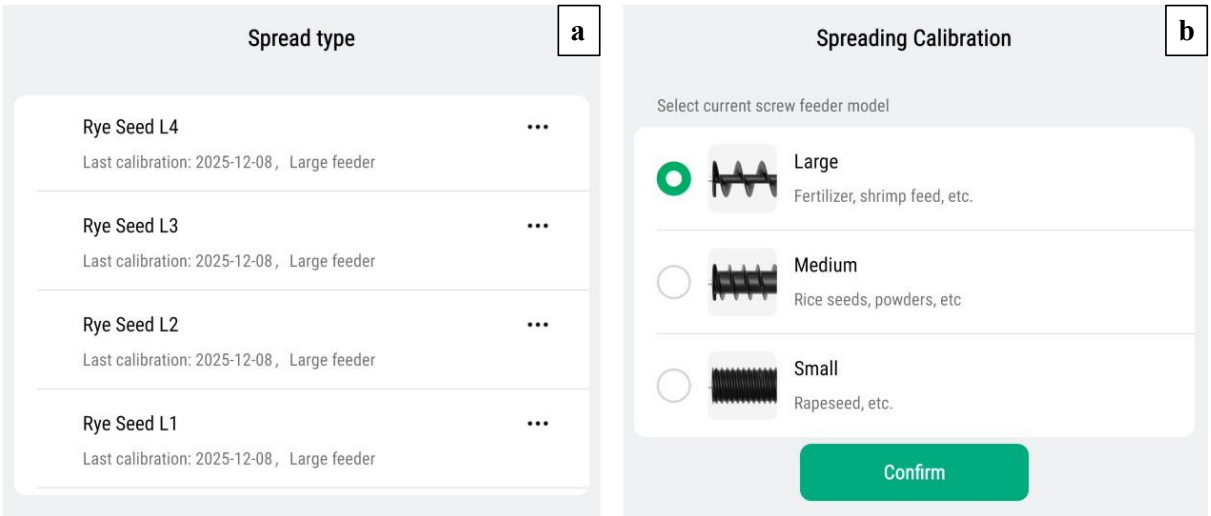

Figure 2.6 a) Material calibration page on the XAG P150 controller and b) Auger selection page that precedes the calibration.

In addition to static testing to calibrate the material flow rate (pounds per minute or kilograms per minute), standard pan testing is also recommended to determine the applied rate and uniformity of material across the swath. The ASABE standard S386.2 outlines the calibration procedure for this testing (ASABE, 2024). The standard provides information on collector size and spacing across the swath, environmental conditions to test in, as well as flight path and test area requirements. In brief, a line of collection pans is established in the field, and the UAS passes are then made over and perpendicular to the collection pans, with material dispensed at the target rate and other desired operational parameters entered into the UAS controller. After each pass, the material collected in each collector is weighed and converted into an applied rate. A coefficient of variation (CV) is calculated to quantify the distribution uniformity of material applied within the swath. This testing to determine the applied rate and spread uniformity is highly recommended to identify the optimal spreading parameters specific to the material being spread and the UAS platform.

2.2 Literature Review

Although limited research is available on the use of modern UAS platforms for spreading cover crops or other dry materials, few recent studies have investigated their application performance and the effect of design characteristics on material distribution within the swath. Thomas (2025) evaluated the accuracy of the metering system and the spreading performance of the DJI T20P using three cover crop mixtures. The author conducted calibration checks by capturing the material from the UAS at multiple set points and determining the flow rate. He found that the internal calibration was appropriate, but there were distinct differences between the manufacturer-recommended and his calibration results. The manufacturer-recommended calibration did not capture a reduction in material flow above 90% of the metering gate opening. It also failed to

determine or provide any information regarding the minimum hopper gate opening for consistent material flow, as the author found distinguishable points at which material flow was inconsistent at lower gate openings. The UAS exhibited a left-skewed single-pass spread pattern, which is inherent to most single-disc broadcast systems. Spread pattern tests conducted at spinner-disc speeds of 550, 800, 1050, and 1300 rpm indicated that the lowest rpm exhibited the highest skewness and the narrowest simulated overlap swath with a CV below 30%. The effect of the other three spinner disc speeds (800, 1050 and 1300 rpm) was not significantly different, though the peaks within the spread pattern decreased with spinner disc speed, and more material was distributed towards the edge of the spread pattern.

Xia et. al. (2025) tested various application heights, flight speeds, and spinner-disc speeds using a DJI Agras T40 for spreading three different granular fertilizer types: small-grain urea (mean particle size of 1.62 mm), large-grain urea (3.49 mm), and urea-ammonium nitrogen (2.92 mm). The authors placed collectors in 5 rows, each with 10 collectors. The rows were 5 m apart, with the pans spaced 1 m within the row. For the parameters examined, a single flight was conducted over the center of the collection area, perpendicular to the rows, with application heights of 2, 3, 4, 5, and 6 m. The authors reported no effect of flight height on distribution uniformity for large granular urea at flight heights below 5 m. At a height of 6 m for large granular urea, the CV value improved to 16.8% and was significantly different from the other tested flight heights. For both small granular urea and urea-ammonium mixed nitrogen, a significant difference in distribution uniformity within the swath was found at a flight height of 2 m for each fertilizer type. For all three granular fertilizers, the application speeds of 2, 4, 6, 7, and 9 m s^{-1} were also tested. The effect of application speed on distribution uniformity was only observed at 5 m s^{-1} for small granular urea and at 2 m s^{-1} for large granular urea. Xia et al. (2025) also tested spinner-disc speeds

of 500, 700, 900, 1100, and 1300 rpm and their effect on spreading performance. A general trend of increasing distribution uniformity with higher spinner disc speed was observed. Although there were no significant differences for the small granular urea, the CV values still improved as the spinner disc speed increased. The authors also examined the course spreading stability (CSS), which represented the material distribution examined 90° to the flight path, moving left to right, and the planar uniformity (PU), which represented the particles caught in each collector compared to the average particle number in each collector. Considering that both the CSS and PU coefficient of variation values generally improved at lower application heights, they recommended applying granular materials at lower heights to reduce the impact of environmental conditions on the spreading performance. They also suggested using higher spinner-disc speeds for all three fertilizers if wider application swaths are desired, with lower speeds more suitable for narrower swaths.

Xunwei et. al. (2024) examined the spreading disc design on a DJI Agras T60 and conducted field tests using urea fertilizer (average particle size of 3.38 mm) and compound fertilizer (2.96 mm) to assess the accuracy of a spread pattern distribution model. The authors performed a simulation test using EDEM 2022.2 software (Altair Engineering, Michigan, USA) and compared the results with field testing conducted utilizing the same parameters. They reported a relative error of 9.18% between the measured and simulated distributions, with the simulation overestimating the amount of fertilizer applied and thus requiring normalization. Given that the simulated results were comparable, the authors proceeded to further modeling and testing using a simulated fertilizer particle size of 2.96 mm. Simulations on spinner-disc designs were conducted at three auger speeds of 100, 300, and 500 rpm, with an analysis examining a static distribution of material around the spreader. Although straight vanes on the spreading disc offered better distribution uniformity at

the lowest material flow rates (auger speed of 100 rpm), curved vanes exhibited improved uniformity at the two highest auger speeds tested. The authors suggested that a combination of the two vane designs (straight and curved) would be ideal for applications, as they can complement each other across a range of material flow rates. Using a similar simulation method for the deflection angle, the authors also examined the curved vane deflection angle at an auger speed of 100 rpm and found that 40° provided the optimal uniformity for the materials tested. The authors used an optimized spreader for a field test examining multiple operational parameters conducted over 3 rows of collectors (spaced 5 m apart), with 17 collectors within each row spaced 0.5 m apart. Keeping all other parameters fixed, individual parameters were tested to determine their effect on the spread distribution. Various spinner-disc speeds (700, 800, 900, 1000, and 1100 rpm), auger speeds (100, 200, 300, 400, and 500 rpm), and flight speeds (3, 5, 7, 9, and 11 m s^{-1}) were tested. Results for effective swath widths of 8, 9, and 10 m suggested that spinner-disc speed had a statistically significant impact on CV values at 9 and 10 m. Auger speed had a significant impact on the CV values across all tested spread widths, as higher speed led to greater deposited material within the swaths. Flight speed significantly affected spread uniformity only at the 8 m spread swath but did not affect the other spread widths tested. The authors also tested three urea application rates of 45, 90, and 135 kg ha^{-1} and three compound fertilizer rates of 150, 225, and 300 kg ha^{-1} using the same sampling method, though with three flights over the area to replicate an overlap application method. They reported that increasing application rates led to lower CV values (38.1, 18.9, and 14.0%, respectively) for the urea, while the CV values across the compound fertilizer rates remained relatively consistent (14.7%, 15.1%, and 17.2%, respectively).

Although few UAS application studies with dry materials were conducted prior to 2024, the rapid advancement of UAS technology has outpaced many of the systems and control mechanisms

used in those studies. As such, the results of those studies remain relevant but must be examined with the understanding that the components and systems discussed are no longer used on prevalent UAS platforms. Song et. al. (2023) examined two commercially available UAS platforms, the DJI T16 and the R20 (Xiangnong Innovation Technology Co., Ltd., Shenzhen, China). The R20 featured a pneumatic air induction system that diverted the gravity-fed dry material into six air ducts, all of which exit the rear in a fan-shaped pattern. The T16 used a more common design: a gravity-fed single-disc spinner spreader. Both UAS were tested with medium granular urea fertilizer. The authors reported that increasing application height generally improved the distribution uniformity of urea as the application swath increased (tested at 5, 7, and 9 m above the collection area). As the application height increased, the distribution of material began to regress from high material peaks near the center of the flight path to flatter material distribution curves. Neither model's system was capable of automatically regulating material flow to compensate for changes in flight speed, which were tested at 2, 4, and 6 m s^{-1}. This inability to regulate material flow led to a decrease in the amount of urea captured as flight speed increased, consistent with previous recommendations that flight speed should be adjusted to target specific application rates with these models.

Wang et al. (2023) designed and tested a 6-channel air-inducted spreader system. The authors conducted initial simulations and design considerations for fertilizer with an average particle size of 2.98 mm. Based on simulated model data, a static collection area with 512 collection pans was developed for the designed spreading system. This static testing was conducted indoors to isolate the system's design influences, with the system placed 5 m above the collection area. The authors found that an optimized version of the system resulted in a slight skewness of material left of the centerline, but simulated overlap CV values were acceptable with (8.7%, 8.8 m swath) and without

(15.3%, 8 m swath) partitions ahead of the 6-channel outlet. They concluded that material flow control from the hopper onto the spreading system can influence the distribution of material in a swath; hence, the improved distribution with partitions that assisted in material flow.

Similarly, Wu et al. (2020) investigated a spreading system for rice seeding with a UAS YRX620 (Guangxi Yunrui Technology Co. Ltd., China). The authors first simulated the distribution uniformity of rice seeds using a bulk material simulation software, EDEM (DEM Solutions, Ltd, Edinburgh, United Kingdom), to determine the application parameters that influence the uniformity of the applied rice seed. It was determined that application height and spinner-disc speed had the greatest effect on the distribution, though baffle ring angle (the angle at which the apron around the spinner disc is flared out) is still influential to a lesser degree. The authors also tested five application heights (0.5, 1, 1.5, 2 and 2.5 m), five spinner disc speeds (400, 450, 500, 550, and 600 rpm), and five baffle ring angles (15˚, 20˚, 25˚, 30˚, and 35˚) within the simulation program. Among the findings, the combination of parameters that yielded the optimal CV value (18.11%) was interpreted as a spinner disc speed of 600 rpm, an application height of 2.1 m, and a baffle ring angle of 26˚. These settings were verified in a static test, in which the CV values ranged from 21% to 39%.

Chapter Three

Application Rate Accuracy and Distribution Uniformity of Cover Crop Seeding with an Unmanned Aerial System (UAS)

3.1 Abstract

The use of unmanned aerial systems (UAS) for seeding cover crops is increasing rapidly, yet limited information is available on their application performance. Therefore, studies were conducted to assess the application rate (metering) accuracy and the distribution uniformity of cover crop seed (cereal rye) applied with a UAS (DJI Agras T25). Static tests were conducted to determine the actual material flow rate from the hopper at different metering gate openings (10% to 100%). Field tests were conducted to determine the applied rate and assess the distribution uniformity of cereal rye across the swath at different target rates and flight speeds. The actual flow rate (kg min^{-1}) differed from the values suggested by the internal calibration, resulting in a significant underapplication of cereal rye (9.5%–17.7%) across different target rates and flight speeds during the field tests. The single-pass spread patterns showed leftward skewness, indicating greater material distribution (51% to 64%) towards the left and less material deposited (29% to 40%) towards the right. The simulated overlap spread pattern analysis indicated no effect of application rate or flight speed on the distribution uniformity of cereal rye. However, the one-direction application method exhibited improved material deposition within the swath than the progressive method. A CV analysis at different simulated effective swaths indicated no considerable improvement in the distribution uniformity at narrower operating swaths. Future research should investigate the effect of other operational parameters, such as application height and spinner-disc speed, on effective swath and uniformity, along with testing different cover crop seeds (mixtures).

3.2 Introduction

The effective use of cover crops in agriculture has been linked to enhanced crop yields, restoration of soil organic carbon (Vendig et al., 2023), reduced soil erosion, and mitigation of nutrient loss through leaching and surface runoff (Kaye & Quemada, 2017). Due to their demonstrated benefits, the use of cover crops among agricultural producers increased by 17% from 2017 to 2022, with over 7.2 million hectares planted (Bowman & Morales, 2024). Typically, cover crops are seeded using a grain drill or broadcast with a spinner-disc spreader; however, these methods can introduce challenges associated with agricultural equipment, such as increased soil compaction (Shaheb et al., 2021) or reduced traction when seeding cover crops in wet field conditions. Another common, though less utilized, method is to broadcast cover crop seed from a manned plane or helicopter. This method is more commonly used when field conditions preclude the use of ground equipment, to establish a cover crop before harvesting a cash crop, or when large fields can be covered more efficiently than with ground equipment. Aerial seeding of cover crops is also subject to challenges, including weather restrictions and an increased risk of off-target seeding due to equipment and environmental turbulence (Wilson et al., 2014).

Recently, the use of Unmanned Aerial Systems (UAS) in agriculture has increased rapidly in the United States, with over 4.1 million hectares treated by UAS in 2024 (ASDC, 2024). The majority of these applications involve applying agrochemicals to agricultural fields or crops. However, most modern UAS platforms also include an interchangeable dry application (spreading) system for broadcasting solid materials such as cover crop seed and small granular fertilizers. These systems typically include a tank, a gravity-fed or auger-type metering mechanism, and a horizontal or vertically mounted spreading mechanism to broadcast material across the swath. Similar metering and spreading systems, particularly single- or dual-disc spinners, are commonly

used on ground-based application equipment to broadcast dry granular fertilizer. Although simple in design, these systems are known to have non-uniform distribution due to their design and the ballistic characteristics of spreading materials (Miclet et al., 2011). To improve application performance, the spreading characteristics of single- and dual-disc broadcast spreaders have been studied by several researchers (Yildirim 2008; Han et al., 2015; Przywara et al., 2020).

With the increased use of UAS for pesticide applications, recent research has focused on understanding their spray performance and the effects of various application parameters on spray efficiency and efficacy (Ahmad et al., 2020; Byers et al., 2024; Güneş & Hasegawa, 2025). These studies have suggested that the proper selection of the application parameters, such as rate, flight speed and height, is important to ensure optimal spray coverage and uniformity. Similarly, improper application of dry materials, particularly cover crops, can have adverse effects, ranging from uneven crop growth to increased seed costs (Bergtold, 2019). Cereal rye (*Secale cereale*) is amongst the most widely used cover crops in the United States (Sever, 2023) due to its numerous benefits, such as excellent winter hardiness, weed suppression, and residue persistence (Basche et al., 2016; Rorick & Kladivko, 2017). In 2023, over 890,000 hectares of cereal rye were planted in the United States (USDA, 2024). Cereal rye is also used in various cover crop mixtures, often seeded with other small grains, legumes, and brassicas. Accordingly, the majority of cover crop seeding with UAS involves broadcasting cereal rye or a cover crop mixture that includes cereal rye. With increased use of UAS for cover crop seeding, investigating their spreading performance, especially application rate and distribution uniformity, is much needed to inform effective utilization of this technology. Therefore, a study was conducted to evaluate the application performance of a UAS for cover crop seeding. The specific objectives of this study were to (1) evaluate the application rate (metering) accuracy of a UAS when applying cereal rye at different

target rates and flight speeds, and (2) assess the distribution uniformity across the swath for cereal rye applied with a UAS at different rates and flight speeds.

3.3 Materials and Methods

3.3.1 Application Equipment and Material

A commercially available UAS, DJI Agras T25 (SZ DJI Technology Co., Shenzhen, China), was used for all experiments conducted in this study. The DJI T25 has a quadcopter arrangement, with a dry material tank capacity of 35 L [Figure 3.1(a)]. A hopper gate (metering disc) with three equally sized slots [Figure 3.1(b)] regulates material from the tank onto a single rotary (spreader) disc, which broadcasts it across a swath. The manufacturer offers three different hopper gate options (small, medium, and large) to meter dry products of varying sizes and densities. Based on preliminary testing, it was determined that a large hopper gate [Figure 3.1(b)] would be adequate to apply the target application rates of cereal rye. The UAS was operated by utilizing a DJI RC Plus remote controller with pre-installed DJI Agras flight planning software. During all field testing, the T25 UAS was connected to the Alabama CORS network to utilize RTK positioning, which resulted in a horizontal and vertical position accuracy of ±10 cm. The DJI flight planning software enabled the creation and utilization of a pre-programmed flight path for conducting all the field tests. The detailed specifications for the DJI Agras T25 UAS are provided in Table 3.1.

Figure 3.1. (a) DJI Agras T25 UAS equipped with the dry spreading system. (b) Large hopper (metering) gate and (c) curved-vane spinner disc used for application of cereal rye with the UAS.

Table 3.1. Specifications for the DJI Agras T25 UAS.

UAS Characteristics	Value(s)
Platform Weight (empty) (kg)	32
Payload (kg)	25
Dimensions (unfolded) (mm)	2585 × 2675 × 780
Tank Volume (L)	35
Hovering Time (full) (min)	6
Recommended Spraying Width (m)	5 – 8
Maximum Spraying Speed (m s^{-1})	10.0
Battery Capacity (mAh)	15,500

Cereal rye seed was used as the cover crop seed for application with the UAS due to its widespread use. A bulk load of cereal rye was acquired in the Fall of 2024, and its bulk and particle density were measured (68.2 kg m^{-3} and 1.2 g cm^{-3}, respectively). The study involved conducting

two different types of tests to accomplish the stated objectives. The first set of experiments to assess the UAS's metering (rate) accuracy included both static laboratory tests and field tests. The second experiment aimed to evaluate the in-swath distribution uniformity of cereal rye and consisted primarily of field tests conducted outdoors at an open, uncropped site.

3.3.2 Static Flow Rate Testing

All static tests were performed at the Biosystems Engineering Research Laboratory located on the Auburn University campus (Auburn, AL). Before any testing, a manufacturer-recommended calibration procedure was performed by filling the tank (80% of the full capacity) with cereal rye and initiating the calibration through the controller. During this calibration, the UAS outputs material at a few different (preset) hopper gate openings and records the flow rate by sensing the material remaining in the tank using an integrated weight sensor. The calibration concludes with a visual graph displaying the flow rate curve (material flow in pounds per minute versus the percentage of hopper opening) for that specific material [Figure 3.2(a)]. This calibration curve can be viewed and saved on the controller for use during field applications. However, it cannot be exported outside the controller and does not provide specific information on flow rate at different hopper openings, except for displaying the maximum flow rate the UAS can achieve at 100% hopper gate opening. Hence, static tests were conducted to determine the actual flow rate (kg min^{-1}) of cereal rye at different hopper gate openings (%) to generate a flow rate curve and compare it with the manufacturer-generated calibration. These tests involved removing the spinner disc from the UAS and supporting it between two raised platforms so that a container could be placed beneath the spreader tank to catch the material dispensed from the hopper, as shown in Figure 3.2(b). Next, the spreader tank was filled with cereal rye, and different gate openings, ranging from 0% to 100% in increments of 10%, were entered into the controller in manual mode [Figure 3.2(c)]. The hopper

gate opening is also referred to as hopper outlet size (%) in the UAS controller. At each opening, the material dispensed from the hopper was collected for 30 seconds and then weighed to determine the flow rate in kilograms per minute. This process was repeated three times at each hopper gate opening.

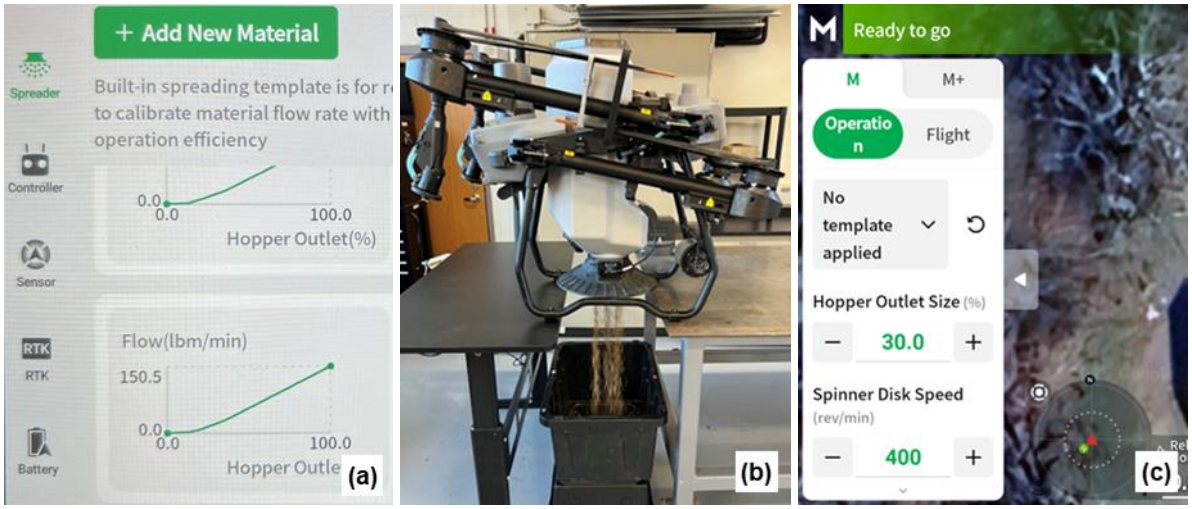

Figure 3.2. (a) Example of flow rate graph generated during calibration, (b) UAS setup for collecting static flow rate data, and (c) UAS controller screen showing the hopper outlet size that was changed during static testing.

The data collected during static testing were plotted with material flow on the y-axis and hopper gate opening on the x-axis to generate a flow rate curve depicting the actual flow of cereal rye across varying hopper gate openings. A least-squares regression curve was fitted to the data in MS Excel to determine the relationship between the measured flow rate and hopper gate opening. Furthermore, Equation 1 was used to calculate the required flow rates to achieve different target application rates and flight speeds during the field tests. This information, along with the flow rate curve, was used to calculate the theoretical hopper gate opening for each target application rate and compare it with the actual hopper gate opening attained by the UAS during field testing.

$$F = \frac{R \times S \times W}{CF} \quad (1)$$

where

F = flow rate (kg min.$^{-1}$)

R = target rate (kg ha^{-1})

S = flight speed (m s^{-1})

W = application swath (m)

CF = conversion factor (167)

3.3.3 Field Testing

Field tests were conducted at the E.V. Smith Research Center in Shorter, AL, on a flat, open, and uncropped site (32°26'39.5" N 85°53'45.5" W). The application area selected within the field for testing was approximately 150 m long and 30 m wide. A flight plan was created in the DJI SmartFarm App, consisting of a single pass of the UAS directly through the center of the application area. This flight plan was used throughout the testing to maintain a consistent single-pass application of the UAS, with all field tests conducted with the UAS in an autonomous 'Route Mode'. During all field tests, the tank level was maintained at 80% of the full capacity (25 kg) by refilling it with cereal rye after each UAS pass. The field tests were conducted in the Fall of 2024 and the Spring of 2025. Table 1 provides information on the different target rates and flight speeds used during field testing. It should be noted that these experiments were not a factorial arrangement of application rate by flight speed but instead were conducted separately during the same week. These tests are labeled Field Test 1 and 2, where Test 1 involved applying cereal rye at rates of 22.4, 33.6, 44.8, 56.0, and 67.3 kg ha^{-1} with the UAS, while keeping the other parameters, including flight speed, height, and spinner disc speed, fixed. Similarly, Test 2 involved applying cereal rye at flight speeds of 6, 7, 8, 9, and 10 m s^{-1} with a fixed application rate, height, and spinner disc speed (Table 3.2). These application rates and flight speeds were selected to produce a varying range of material flow rates, enabling an accurate evaluation of UAS metering accuracy and

distribution uniformity. Along with the fixed application height of 3.8 m and spinner disc speed of 1000 RPM, these parameters also represented the nominal application rates (33.6 - 44.8 kg ha^{-1}) and flight speed (10 m s^{-1}, which represented the maximum speed) used by the UAS operators for broadcasting cover crop seed. The application parameters, such as target rate, speed, height, and spinner speed, specific to each test, were entered into the controller before each flight.

Table 3.2. Application parameters specific to each field test conducted for assessing UAS seeding performance.

Field Test	Rate (kg ha^{-1})	Speed (m s^{-1})	Height (m)	Spinner Speed (RPM)
1	22.4	10	3.8	1000
	33.6	10	3.8	1000
	44.8	10	3.8	1000
	56.1	10	3.8	1000
	67.3	10	3.8	1000
2	44.8	6	3.8	1000
	44.8	7	3.8	1000
	44.8	8	3.8	1000
	44.8	9	3.8	1000
	44.8	10	3.8	1000

3.3.4 Application Rate Assessment

During field testing, the first experiment involved removing the spinner disc and attaching a rectangular collector, measuring 61 cm × 41.3 cm × 15.2 cm, underneath the UAS to collect the material dispensed from the hopper during the flight. This data collection was performed across different target rates and flight speeds (Table 3.2.), with each test replicated four times and each flight constituting a replication. After each flight, the collector was removed and weighed using a scale with a readability of 0.01 g (Ohaus Courier 5000, Ohaus Corporation, Parsippany, New Jersey) to determine the total amount of material (cereal rye) dispensed by the UAS. Based on the fixed application area (0.105 ha) used for all field tests, the theoretical amount of material to be applied by the UAS was also calculated for each target application rate. The theoretical and actual

values were compared to evaluate the UAS's metering accuracy. The hopper gate opening (%) attained by the UAS (displayed on the controller during each flight) was also recorded during field tests to enable comparison with the theoretical gate opening (%) determined during the static flow rate testing.

3.3.5 Distribution Uniformity Assessment

After completing field tests without the spinner disc, the second experiment involved reattaching the spinner disc to the UAS and capturing the applied material in collection pans placed on the ground. Before this data collection, preliminary tests were conducted using five different collection pans that varied in size, particularly in terms of collector opening and depth. This testing was performed to select the collection pan that captured the most material and with a minimal seed bounce out of the pan. Based on this testing, the collection pans measuring 61.8 cm × 45.6 cm × 26.8 cm (shown in Figure 3.3) were selected for this set of field data collection. A rectangular piece of Styrofoam was also placed at the bottom of each pan to further prevent any material from bouncing out. All field tests for assessing the distribution uniformity of cereal rye were conducted following the procedures outlined in the ASABE standard S386.2, Calibration and Distribution Pattern Testing of Agricultural Aerial Application Equipment (ASABE, 2024), unless otherwise noted. A total of 29 pans, spaced evenly at 0.61 m intervals from the center of one pan to the next, were placed in a single line within the application area (Figure 3.3). This arrangement of pans was perpendicular to the flight path and was directly centered under the UAS pass. The total distance covered by the pans was 17.7 m, which was more than twice the spread swath (5 to 8 m) recommended for the UAS manufacturer. During each test, the UAS performed a single pass over the collection pans with the desired application parameters preset in the controller and broadcast the material within the application area.

Figure 3.3. Data collection setup demonstrating the collection pans placed within the application area and perpendicular to the UAS pass for assessing the distribution uniformity of cereal rye across the swath.

After each flight, the material from each pan was carefully collected in a small, pre-labeled zip-lock bag and stored in a large container to be weighed later. During field testing, a weather station (6252 Vantage Pro2, Davis Instruments, Hayward, CA) was installed within the application area to record meteorological conditions, including wind speed and direction, temperature, and relative humidity, in 1.0-minute intervals. The weather station was installed at a height of 1.8 m from the ground and was located approximately 10.0 m away from the outermost collection pan towards the left side of the swath. The meteorological data averaged for the duration of each field test are presented in Table 3.3. The weather conditions stayed consistent throughout the field testing, with the wind speed remaining mostly low (<1.9 m s^{-1}) during both field tests, resulting in no significant effect on the application of cereal rye. The wind direction was north to northeast and stayed within ±15˚ perpendicular to the orientation of the collection pans throughout the testing.

Table 3.3. Meteorological conditions recorded during field tests conducted for assessing the distribution uniformity of cereal rye applied with the UAS. Values represent mean ± standard deviation.

Field Test	Wind Speed ($m\ s^{-1}$)	Temperature (˚C)	Relative Humidity (%)
1	1.4 ± 0.5	11.4 ± 0.2	71.5 ± 1.3
2	1.2 ± 0.3	14.0 ± 0.2	62.9 ± 0.6

3.3.6 Data Analysis

The material collected during the field tests was weighed using a scale with a readability of 0.01g (Ohaus Scout SPX222, Ohaus Corporation, Parsippany, New Jersey) and recorded in an MS Excel sheet. These weights were converted into an applied rate in kilograms per hectare at each pan location within the swath (ASABE S386.2). Further, single-pass and overlap simulated distribution patterns were generated from the applied rate calculated at each pan location. The single-pass patterns were generated by plotting the mean applied rate ($kg\ ha^{-1}$) versus the location of each pan within the swath. To analyze and compare the single-pass patterns, total material applied within the swath (kg), maximum single-pass swath (m) and pattern skewness (%) were calculated and subjected to analysis of variance (ANOVA) using an alpha value of 0.05. Treatment means for significant effects were separated using the Student's t-test ($p \leq 0.05$). The overlap spread patterns, characterizing the uniformity of distribution within the swath, were generated for an effective swath of 7.3 m (24 ft), which represented the nominal route spacing (7 – 7.5 m) used by the UAS applicators for cover crop seeding. To evaluate and compare the effect of application method on the distribution uniformity of cereal rye, simulated overlap passes were generated using two different methods – progressive and one-directional – as defined in the ASABE Standard S386.2 (ASABE, 2024). The progressive method, as the name suggests, uses a progressive application pattern, with the direction of travel changing from pass to pass. This produces a right-on-right wing overlap that alternates with a left-on-left wing overlap. The one-direction (also

known as racetrack) method results in a right-on-left wing overlap pattern. For all simulated overlap patterns, the mean applied rate and coefficient of variation (CV), which indicates the amount of variability within the swath, were computed using equations in ASABE S386.2 (ASABE, 2024).

3.4 Results and Discussion

3.4.1 Application Rate Assessment: Static Testing – Flow Rate Calibration

The flow rate curve generated from the data collected during the static testing is presented in Figure 3.4(a). It depicts a non-linear relationship between the amount of material flow per minute (kg min^{-1}) and the hopper gate opening (%). The trendline fitted to the data provided a quadratic equation (Equation 2) with an R^2 value of 0.99.

$$F = 0.009X^2 + 0.048X \qquad (2)$$

Where F is the flow rate in kg min^{-1} and X is the percent hopper opening.

Using this equation, the maximum flow rate for cereal rye (at 100% hopper gate opening) was determined to be 94 kg min^{-1}. This value differed significantly from the maximum flow rate of 68.3 kg min^{-1} (150.5 lbm min^{-1}), displayed on the controller at completion of the manufacturer-recommended calibration procedure [Figure 3.4(b)]. The manufacturer-generated calibration curve [Figure 3.4(b)] also visually differed from the actual flow rate curve [Figure 3.4(a)], where it appears to show a linear relationship – instead of the quadratic relationship as noted earlier – between the flow rate and gate opening, especially between the gate opening of 20% to 100%. These differences in flow rates highlight the inadequacy of the manufacturer's calibration procedure in accurately representing the actual flow rate from the hopper and would likely result in significant rate errors during the application of cereal rye with the UAS. Considering these results, similar calibration issues can also be expected for other cover crop seeds or mixtures, as

the main problem lies in the calibration approach (using only three to four measurements) used by the manufacturer, which fails to account for and depict the non-linear (or quadratic) relationship between the hopper gate opening and material flow rate. The authors believe that adding more measurement points (likely three to four additional evenly spaced measurements) to the existing calibration procedure can improve its accuracy and enable more precise applications. Additionally, it is worth noting that the current calibration does not account for product density and only estimates material flow through different openings. The ability to include and account for product density during calibration can further improve the UAS's metering accuracy.

Thomas (2025) performed similar calibration testing with different cover crop seeds, including cereal rye, using the DJI Agras T20P UAS (SZ DJI Technology Co., Shenzhen, China), which has a similar gravity-fed hopper gate opening as the DJI Agras T25. The author also noted some limitations of the UAS's self-calibration process. Unlike the DJI T25, the T20P UAS does not provide any information on the maximum flow rate, which means the operator cannot compare or verify the accuracy of the flow rate determined through the calibration process. Song et al. (2020) compared the fertilizer discharge (flow rates) from four different UAS models equipped with different metering systems. The authors reported that the relationship between the discharge rate and opening or angle of the metering gate was specific to each system and varied from a perfect linear regression for one metering system to a quadratic relationship for other systems. The authors also emphasize that determining an accurate flow rate response for the existing metering system on the UAS is crucial for achieving the desired rates, particularly for precise variable-rate applications.

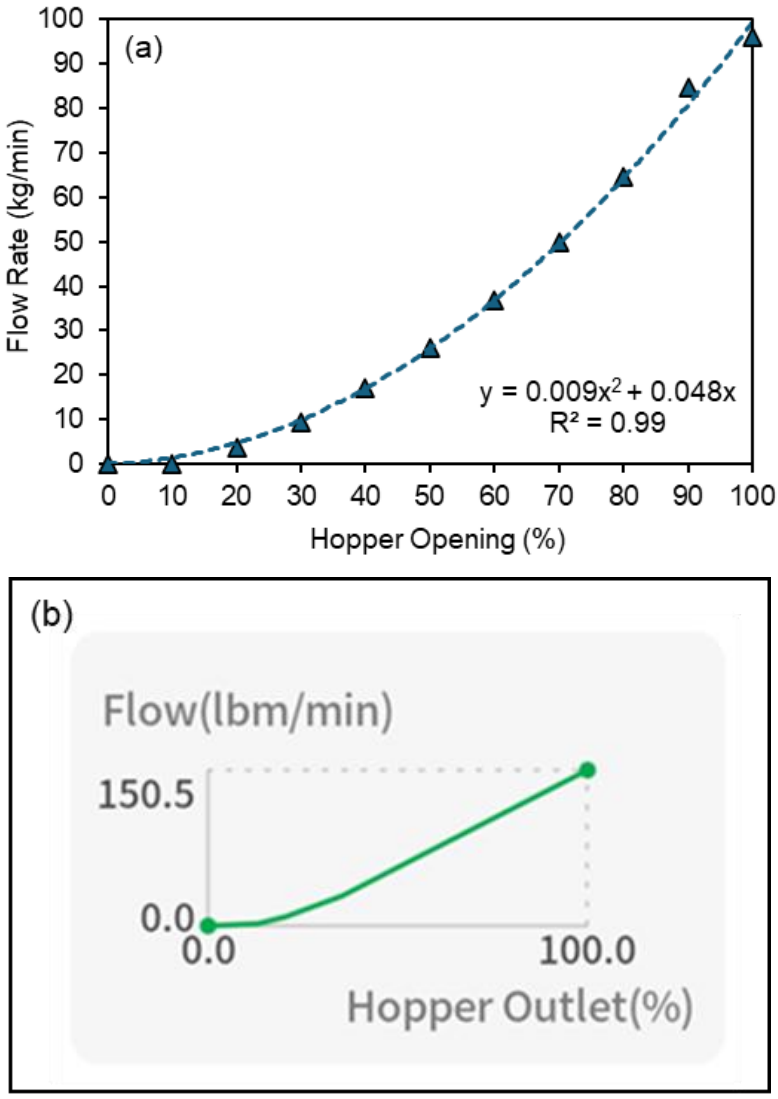

Figure 3.4. (a) Flow rate versus hopper opening (%) curve generated from the data collected during static testing. (b) Graph showing the flow rate versus hopper opening based on the manufacturer-recommended calibration.

3.4.2 Application Rate Assessment: Field Testing

The summarized data from the field testing conducted to assess the accuracy of the application rate (without the spinner disc) are presented in Table 3.4. For each target rate, the theoretical gate opening was determined by calculating the required flow rate to achieve that rate and then using the quadratic equation from the flow rate curve shown in Figure 3.4(a). It can be observed that the actual hopper gate opening attained by the UAS (as recorded by the flight controller during

application) was approximately 2% to 4% less than the theoretical hopper gate opening. Consequently, differences between the target and measured rates were also observed, with under-application ranging from 9.5% to 17.7% across the various application rates and flight speeds. Interestingly, the highest under-application (17.2%–17.5 %) across both field tests was observed at the lowest target rate (22.4 kg ha^{-1}) and the lowest speed (6 m s^{-1}), and was significantly greater than the under-application (9.5%–12.9%) observed across the other rates and speeds. Considering the trapezoidal shape of the hopper gate and the oblong shape of cereal rye seeds, this may be attributed to material bridging occurring at the lower gate openings, especially below 30%, resulting in an inconsistent material flow through the hopper opening. This inconsistent material flow at the lower gate openings (<30%) was also visually observed during the static flow testing. While that effect may not be as pronounced during the flight due to vibration induced by the propellers and the slight forward tilt of the UAS, a significantly low under-application observed at the lowest target rate and flight speed suggests potential metering issues under these application conditions and warrants further investigation. Thomas (2025) also reported similar issues during testing with different cover crop seeds and suggested determining a minimum hopper gate opening (%) specific to the material being spread (based on seed size and shape) to ensure consistent material flow. Considering these observations, it is worth mentioning that the proper selection of a hopper metering gate, based on the type of cover crop seed and the target application rate, is important for consistent material flow and accurate applications with UAS. Overall, the findings from these field tests further validate the calibration issues discussed earlier and underscore the importance of proper calibration for accurate metering and applying the desired rate of cover crop seed with the UAS.

Table 3.4. Data summary from the field tests involving cereal rye dispensed from the UAS (without the spinner disc) at different application rates and flight speeds.

Field Test	Target Rate (kg ha^{-1})	Flight Speed (m s^{-1})	Gate Opening (%)		Measured Rate[a] (kg ha^{-1})		Percent Difference[a], [b] (Actual – Target)
			Theoretical	Actual	Mean	Std. Dev.	
1	22.4	10	29.5	25.8	18.5 a	0.9	-17.2 a
	33.6	10	36.7	34.8	30.4 b	0.8	-9.5 b
	44.8	10	42.7	39.8	40.1 c	1.1	-10.5 b
	56.0	10	48.1	46.0	49.4 d	0.4	-11.8 b
	67.3	10	52.9	51.5	60.1 e	1.1	-10.7 b
2	44.8	6	32.5	29.8	36.9 A	1.3	-17.7 A
	44.8	7	35.3	33.3	39.2 A	3.2	-12.5 B
	44.8	8	37.9	34.5	39.2 A	2.3	-12.5 B
	44.8	9	40.4	37.0	39.0 A	1.3	-12.9 B
	44.8	10	42.7	39.8	40.1 A	1.1	-10.5 B

[a] Values followed by the same letters within each column and field test are not significantly different from each other ($p>0.05$).

[b] Negative values indicate under-application.

3.5 Distribution Uniformity Across the Swath

3.5.1 Single-Pass Spread Patterns

The single-pass spread patterns for cereal rye applications at different rates and flight speeds are presented in Figure 3.5(a) and 3.5(b), respectively. A common trend across the spread patterns was a peak indicating heavy material deposition to the left, between -1.0 and -2.0 m within the swath. The observed skewness in the spread patterns is a typical characteristic of single-disc broadcast systems (Cunningham, 1963; Davis and Rice, 1973; Han et al., 2015). A single-disc system with clockwise rotation usually deposits most of the material to the left of the swath, due to the rotational forces enacted on the material as the spinner disc rotates. Another noticeable trend in the spread patterns was the presence of a second, much smaller, peak to the right of the UAS centerline, approximately at 1.8 m within the swath. Across single-pass patterns at different application rates, the shape of the spread patterns remained relatively similar, with magnitude increasing with the application rate [Figure 3.5(a)]. In contrast, the single-pass patterns across

different flight speeds mostly overlapped, indicating consistent cereal rye deposition within the swath, regardless of the increase in flight speed.

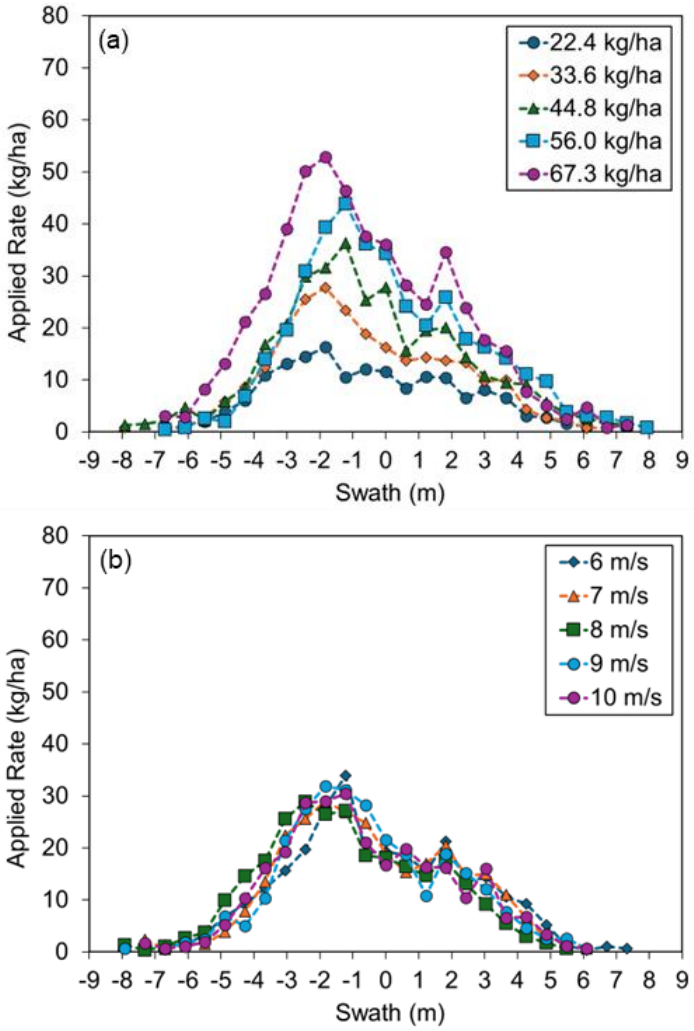

Figure 3.5. Single-pass spread patterns for cereal rye applied with the UAS at different (a) application rates, and (b) flight speeds. 0 m on the x-axis represents the center of the UAS flight path.

The summary statistics for single-pass patterns, including total mass collected within the swath, maximum single-pass swath and skewness, are presented in Table 3.5. The total mass (i.e., the total amount of cereal rye deposited within the swath) increased significantly with increasing target rate, as expected due to higher flow rate (kg min^{-1}) as the rate (kg ha^{-1}) increased. In contrast, the total mass was similar across the different flight speeds, indicating that the same amount of

cereal rye was deposited within the swath regardless of an increase in the flight speed from 6 m s^{-1} (60% of the maximum speed) to 10 m s^{-1} (maximum speed). The maximum single-pass spread swath ranged from 11.9 to 13.6 m across different rates and flight speeds. Interestingly, the spread swath at the 44.8 kg ha^{-1} was significantly wider (approximately 1.5 m) than at the lowest and highest rates of 22.4 and 67.3 kg ha^{-1}. Conversely, the maximum single-pass swath was similar across the flight speeds, ranging from 11.9 to 12.8 m. In terms of skewness, the data confirmed the leftward skew observed in the single-pass patterns (Figure 3.5), with 51% to 64% of cereal rye (by mass) deposited on the left side of the swath and 33% to 40% on the right. Statistical analysis also indicated greater skewness in the single-pass pattern at the 67.3 kg ha^{-1} rate than at the 56.0 kg ha^{-1} rate. Similarly, the single-pass pattern at 8 m s^{-1} flight speed showed greater leftward skewness than those at 6 and 7 m s^{-1}. Overall, the results obtained here were consistent with those of other researchers, with similar skewness observed in single-pass patterns when applying granular fertilizer (Song et al., 2020; Song et al., 2023) and cover crop seed (Thomas, 2025) with a UAS equipped with a single-disc broadcast spreading system.

Table 3.5. Summary statistics for the single-pass spread patterns for cereal rye applied with a UAS at different application rates and flight speeds.

Field Test	Target Rate (kg ha^{-1})	Flight Speed (m s^{-1})	Total Mass[a] (kg x 10-3)	Maximum Swath[a] (m)	Skewness[a], [b] (%, L/R)
1	22.4	10	3.7 a	12.2 b	56/37 ab
	33.6	10	5.8 b	12.9 ab	59/34 ab
	44.8	10	7.9 c	13.6 a	57/35 ab
	56.0	10	8.7 d	12.7 ab	51/40 b
	67.3	10	11.3 e	12.0 b	60/33 a
2	44.8	6	8.1 A	12.8 A	54/39 A
	44.8	7	8.2 A	12.2 A	56/37 A
	44.8	8	8.0 A	11.7 A	64/29 B
	44.8	9	8.2 A	12.1 A	60/33 AB
	44.8	10	8.0 A	11.9 A	59/35 AB

[a] Values followed by the same letters within each column are not significantly different from each other ($p>0.05$).

[b] Negative values indicate under-application

3.5.2 Simulated Overlap Spread Patterns

The simulated overlap patterns in Figures 3.6(a) and 3.6(c) show that the progressive application method resulted in a greater material deposition on the left side of the UAS centerline than on the right, leading to greater variability in material distribution within the swath. This also implies that the more skewed the single-pass pattern is, the greater the amount of variability in material deposition when using this method. Conversely, the overlap patterns in Figures 3.6(a) and 3.6(c) (based on the one-direction application method) show a more even distribution of material across the swath than those of the progressive method. This can also be explained by the fact that, in the one-direction method, the peaks with greater material deposition overlap with the valleys representing lower material distribution, thereby providing a more even material distribution within the swath. It should be noted that the UAS (DJI Agras T25) used in this study currently offers only a progressive application method as the default option during flight planning. However, other UAS models with similar (single-disc) dry spreading systems, such as the DJI Agras T30, offer an option to lock the UAS orientation, enabling the system to perform an application similar to the one-direction method. Several UAS models from other manufacturers also currently offer this option, and it is likely that, with further developments in UAS technology, most commercial platforms in the future will be available with the option to customize the flight plan, configure the UAS flight pattern, and adjust other application parameters.

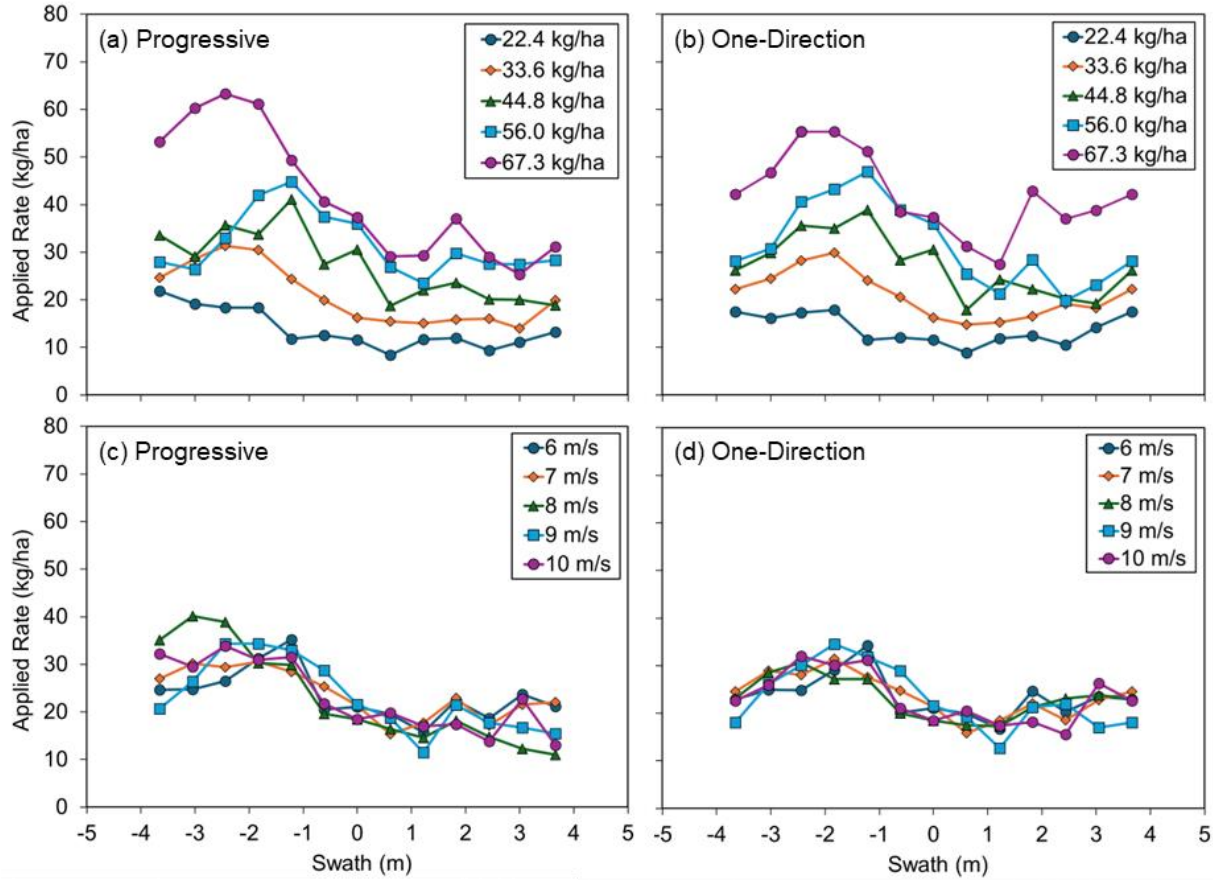

Figure 3.6. Simulated overlap spread patterns generated using progressive and one-direction application methods for cereal rye applied with the UAS at different rates (a & c) and flight speeds (b & d).

Table 3.6 presents the summary statistics for simulated overlap patterns, including the mean applied rate and CV (representing the variability in material distribution across the swath). It can be observed that the mean applied rate is similar across application methods despite observed visual differences in simulated overlap patterns. This was because the same amount of material is applied/distributed across the effective swath, regardless of the application pattern (left-on-left [progressive] or left-on-right [one-direction]). Additionally, the mean rate was considerably lower than the target rate, ranging from 33.9% to 44.3% across different application rates and flight speeds. This large difference between the target and measured can be attributed to two reasons. The first being the under-application by the UAS's metering mechanism itself, which was

determined to be between 10.6% and 17.7% (Table 3.4). The other reason concerns the efficiency of collectors. The collection pans used during field testing were assumed to have 100% collection efficiency, although it is known that solid, dry materials can bounce in and out of collection pans (Parish, 1991). This resulted in less material being collected in the pans than dispensed by the UAS, thereby leading to a lower measured rate. A comparison of the data in Table 3.4 and Table 3.6 suggests that the difference between the material dispensed by the UAS and collected in the pans ranged from approximately 17% to 33%, which can be attributed to the inefficiency in the measurement approach and/or the collection pans. Accurately determining collector efficiency is important, yet a challenging task as the collector's performance is dependent on several factors, including the material being applied and its physical properties, collector design, height of the collectors, wind conditions, and field/ground surface conditions (Whitney et al., 1987; Parish, 1991; Thomas, 2025). However, there is a need to investigate practical methods for determining collector efficiency in aerial application of dry materials.

Table 3.6. Mean Rate and CV calculated from the simulated overlap pattern data for the application of cereal rye with a UAS at different target rates and flight speeds.

Field Test	Target Rate (kg ha^{-1})	Flight Speed (m s^{-1})	Progressive[a]		One-Direction[a]		Difference (%) (Mean – Target)
			Mean Rate (kg ha^{-1})	CV (%)	Mean Rate (kg ha^{-1})	CV (%)	
1	22.4 a	10	13.7 e	30	13.7 e	22	-38.4
	33.6 a	10	20.8 d	30	20.8 d	23	-38.1
	44.8 a	10	27.3 c	27	27.3 c	24	-39.1
	56.1 a	10	31.2 b	21	31.2 b	28	-44.3
	67.3 a	10	41.0 a	33	41.0 a	20	-39.1
2	44.8 A	6	29.1 A	22	29.1 A	19	-35.0
	44.8 A	7	29.5 A	22	29.5 A	19	-34.2
	44.8 A	8	28.8 A	39	28.8 A	19	-35.7
	44.8 A	9	28.9 A	33	28.9 A	28	-35.5
	44.8 A	10	29.6 A	32	29.6 A	24	-33.9

[a] Values followed by the same letters within each column are not significantly different from each other ($p>0.05$).

For distribution uniformity, the CV values ranged from 21% to 39% across different rates and speeds for the progressive method, and from 19% to 28% for the one-direction method. Within each application method, statistical analysis indicated that neither application rate nor flight speed had a significant effect on the distribution uniformity of cereal rye within the swath. Song et al. (2023) reported similar findings, in which flight speed (and application height) did not affect the in-swath distribution uniformity of urea applied with a UAS equipped with a single-disk spreading system. It is important to note that most UAS applications occur at maximum flight speed to increase field efficiency. The results obtained here suggested that applications at lower flight speeds did not improve the uniformity of cereal rye distribution within the swath.

A comparison among application methods indicated that the one-direction method exhibited improved distribution uniformity than the progressive method across both application rates and flight speeds (Table 3.7). On average, the mean CV values for the one-direction method were approximately 5% to 7% lower than the progressive method. Grift (2000) reported that the skewness of material spread – an inherent design characteristic of a single-disc spreader – can negatively impact CV values for overlap spread patterns, especially when using a progressive application method. Similar results were obtained in the present study, where the leftward skew in the single-pass spread patterns led to greater variability in the progressive application method than in the one-direction method. This can be an important consideration for operators seeking to minimize in-swath variability, especially when using UAS capable of configuring the application pattern.

Table 3.7. CV values for simulated overlap patterns for progressive and one-direction application methods.

Field Test	Test Parameter	Application Method	CV (%)
1	Rate	Progressive	28 a
		One-Direction	23 b
2	Speed	Progressive	29 A
		One-Direction	22 B

3.6 Distribution Uniformity at Different Effective Swaths

For application of granular fertilizer with broadcast spreaders, a CV value of 20% or less is typically considered acceptable (Fulton et al., 2005). However, previous studies have suggested CV values between 20% and 30% are more reasonable for fertilizer applications with broadcast spreaders under real-world field conditions (Crozier & Roberson, 2014; Song et al., 2020). Similarly, the acceptable CV value for aerial applications is likely to be close to 30%, especially for UAS applications with single-disc broadcast systems. Though most commercial operators use wider swaths (7 to 9 m) for seeding cover crops, the manufacturer recommends adjusting the parameters to achieve a spread swath of 5.0 to 7.0 m. To examine whether the distribution uniformity of cereal rye can be improved by reducing the effective swath, CV values at different effective swaths were computed for both progressive and one-direction application methods, and are presented in Table 3.8.

For the progressive application method, the CV values at the reduced effective swaths of 4.9 and 6.1 m were mostly similar (within 5% to 6%) to those obtained at the 7.3 m effective swath across most parameters. Except for the CV value at the 56.1 kg ha^{-1} rate, the 3.7 m effective swath showed improvements in CV across most application rates and flight speeds. However, a narrower swath may not be practical, as it would significantly reduce field efficiency and require considerably more tank refills. The one-direction method generally showed improved CV values

(<30% across all rates and flight speeds) compared to the progressive application, with distribution uniformity further improved (CV <20%) at the 3.7 effective swath. Thomas (2025) observed similar results with cereal rye applications using the DJI T20P UAS, with CV values below 20% at narrower effective swaths. The author also noted that narrower effective swaths (below 6-7 m) may not be practical for commercial applications. Overall, these findings suggest that CV values of 30% or less may be more common and considered acceptable for cover crop applications with UAS. Further improvement in distribution uniformity may be obtained by adjusting other operational parameters, such as spinner disk speed and/or application height.

Table 3.8. The coefficient of variation (CV) values at different effective swaths for progressive and one-direction application methods across different application rates and flight speeds.

Effective Swath (m)	Coefficient of Variation (%)									
	Target Rate (kg ha^{-1})					Flight Speed (m s^{-1})				
	22.4	33.6	44.8	56.1	67.3	6	7	8	9	10
	---------- Progressive Application ----------									
3.7	17	25	26	28	21	20	19	20	28	25
4.9	29	34	30	25	34	20	28	33	33	35
6.1	32	35	28	18	36	24	28	39	31	34
7.3	30	30	27	21	33	22	22	39	33	32
	---------- One-Direction Application ----------									
3.7	11	8	9	9	11	12	8	10	14	6
4.9	15	20	17	17	16	18	21	18	22	18
6.1	22	24	21	23	18	22	25	20	23	24
7.3	23	23	24	28	20	19	19	19	28	24

A few limitations to this study should be noted and considered for future experiments. Most seeding experiments were conducted on calm days with low wind conditions, whereas most commercial seeding applications occur in variable wind conditions. Wind speed and direction can considerably affect the distribution pattern of cereal rye (and other cover crop seeds). Therefore, the in-swath variability could be much higher in real-world application conditions than observed

in the current study. Additionally, all data in this study were collected during single-pass applications with the UAS, whereas the commercial applications involve multiple passes within the field, which could possibly result in different applied rates and distribution across the swath than those achieved by analyzing the simulated overlap pass spread patterns. Hence, it would be valuable to assess and validate the accuracy of the applied rate and the uniformity of distribution in large-scale fields during UAS seeding applications. Future studies on UAS seeding performance should also investigate the effect of other operational parameters, such as application height and spinner-disc speed, as they can influence both effective swath and distribution uniformity.

3.7 Conclusions

Static and field experiments were conducted to assess the accuracy of application rate and distribution uniformity of cereal rye applied with a commercial UAS (DJI Agras T25) at different rates and flight speeds. The actual material flow rate differed from the manufacturer-recommended calibration, resulting in the measured (cereal rye) application rate being 9.5% to 17.7% lower than the target rate across different rates and flight speeds. Results also indicated issues with consistent material flow (due to bridging) at lower hopper gate openings (%), underscoring the need for proper metering gate selection based on the target application rates and the type of material being spread. The single-pass distribution patterns for cereal rye showed leftward skew, with maximum swath widths ranging from 11.9 to 13.6 m across different application rates and flight speeds. The simulated overlap pattern analysis exhibited CV values ranging from 19% to 39% and no significant effect of application rate and flight speed on the distribution uniformity of cereal rye within the swath. However, the one-direction application method demonstrated more uniform deposition across the swath than the progressive application pattern. A comparative analysis of CV values at different effective swaths suggested no considerable improvement in distribution

uniformity for applications at narrower (and less practical) operating swaths compared to the wider swath (7.0 m) commonly used by UAS operators.

Chapter Four

Effect of Operational and Structural Parameters on Spreading Distribution of Cover Crop Seed (Cereal Rye) Applied with a UAS

4.1 Abstract

With the increased use of unmanned aerial systems (UAS) to spread cover crop seed in recent years, there is a need to determine the effects of operational parameters and the dry spreader components on application performance. Therefore, studies were conducted to investigate the effects of application height (3.0, 3.8, and 4.6 m) and spinner-disc speed (700, 1000, and 1300 rpm) on the distribution uniformity of cover crop seed (cereal rye) applied with a commercial UAS (DJI Agras T25). Additionally, the effects of hopper metering gate design (medium and large) and spinner-disc design (straight and curved vanes) on material distribution were evaluated at 22.4, 33.6, & 44.8 kg ha^{-1} for the metering gates and 33.6, 44.8, & 56.0 kg ha^{-1} for the spinner discs. Results showed that both application height and spinner-disc speed affected cereal rye distribution within the swath, with single-pass spread patterns showing lower material deposition at an application height of 4.6 m and a spinner-disc speed of 700 rpm compared to other heights and speeds. Similarly, the maximum single-pass swath increased with application height from 11.0 to 13.4 m, and for spinner-disc speed from 10.2 to 14.5 m. The overlap spread patterns exhibited similar distribution uniformity across application heights (CV = 30 – 33 %), whereas the spinner-disc speeds of 1000 and 1300 rpm (CV values of 31 and 26, respectively) demonstrated improved spreading uniformity compared to the 700 rpm (CV = 38%). The medium metering gate showed a wider single-pass swath than the large gate, but the mean applied rate and distribution uniformity were similar across the two gate designs. Similarly, the spinner-disc with curved vanes exhibited greater material deposition, a wider single-pass swath, and greater leftward skewness than the

straight-vane disc; however, the overlap spread patterns showed comparable spreading distribution (CV = 29 – 34 %) across both spinner-disc designs.

4.2 Introduction

The use of Unmanned Aerial Systems (UAS) in global agricultural production systems has increased rapidly within the last decade. While UAS technology originated in Asia and has been used throughout Asian agriculture for nearly forty years (He et al., 2017; Gohari et al., 2023), it has seen an increased adoption in agriculture in the United States in recent years, with over 4.1 million hectares of agricultural land treated in 2024 (ASDC, 2024). This can be attributed to many factors, including the availability of commercial platforms, increased payload capacity, and high-efficiency propulsion systems. Initially, UAS were primarily used to apply agrochemicals, such as fungicides and herbicides, offering benefits similar to traditional aerial applications while providing greater maneuverability than ground-based equipment (Zhang et al., 2023). However, their use for applying small, dry solid materials, especially cover crop seed, has increased rapidly, as most commercial UAS platforms are equipped with interchangeable dry spreading systems. The spreading system on a UAS typically consists of a tank with a gravity-fed or auger-type metering mechanism, along with one or more horizontally or vertically oriented disc(s) to broadcast the material. The most common type of broadcast system on commercial UAS utilizes a single rotating disc with vanes to spread material across the swath, similar to some variants of ground-based single-disc fertilizer spreaders.

Spinner-disc type broadcast spreaders have been used in agriculture for many years due to their simple operation, low maintenance costs, and reliable design (Han et al., 2019). Several researchers have investigated the spreading characteristics of rotary broadcast spreaders, especially single-disc, with many studies focusing on the effect of different operational parameters on

material distribution within the swath (Cunningham, 1963; Glover & Baird, 1973; Davis & Rice, 1974). These studies reported that single-disc spreaders typically broadcast more material in the direction of disc rotation, resulting in a skewed distribution pattern (Miclet et al., 2011). In comparison, dual-disc broadcast spreaders were found to provide better distribution uniformity, and as such, their use is continued on modern fertilizer application equipment. For both single- and dual-disc spreaders, the effects of vane shape, feeder gate design, and spinner disc RPM have also been evaluated and found to affect distribution within the spreading swath. (Yildirim, 2011; Fulton et al., 2020). Several researchers have also used computer modeling to simulate the material flow and distribution by single- and dual-disc fertilizer spreaders in an effort to determine optimal operational parameters and disc designs. (Grift, 2000; Hall et al., 2010; Pryzywara, 2020). In addition to application parameters, the distribution uniformity of dry solid materials applied with rotary spreaders is also influenced by material properties such as particle size, bulk density, and shape. (Hofstee and Huisman, 1990; Virk et al., 2013). A larger, heavier particle usually results in a wider possible swath, while spherical particles have lower aerodynamic resistance and thus can travel farther than irregularly shaped particles (Hofstee, 1992). While significant research has been conducted on evaluating the spreading performance of ground-based fertilizer spreaders, the application performance and the effects of different operational parameters on material distribution have not been investigated for UAS spreaders. As such, research on dry spreading systems for UAS is limited, with only a limited number of studies (Sizemore, 2026, Thomas, 2025, and Xia, 2025) conducted to date. These studies have investigated operational parameters on dry materials including cover crop seed and fertilizer, though each study has examined different generations of commercially available UAS platforms. With technological advancements on each generation of

UAS, it is critical that these advancements are understood so appropriate parameters can be used for effective applications.

The use of UAS for seeding cover crops offers several advantages over traditional ground or aerial seeding methods. Some drawbacks inherent to ground-based equipment, such as soil compaction, crop damage, and traction issues, can be partially mitigated by using UAS. Modern UAS platforms offer similar benefits to those of manned aircraft, but without many of the dangers or risks associated with increased collision risk or off-target applications (NTSB, 2014; Wilson et al., 2014). The rapid growth of UAS for seeding cover crops necessitates understanding their spreading performance, specifically the effects of different operational and structural (design) parameters on material uniformity within the swath. Rapid adoption within the industry, but few research studies, has led to a gap in understanding the application performance of these UAS. Therefore, a study was undertaken to evaluate the application performance (material distribution within the swath) of a UAS when applying cover crop seed. Cereal rye (*Secale cereale*) was selected as the cover crop seed due to its extensive use as a stand-alone crop as well as in different mixtures with legumes, grains, or grass seeds. In 2023, over 890 thousand hectares of cereal rye were planted in the United States (USDA, 2024), not including any cover crop mixtures that utilize cereal rye as a part of the product. In this study, the effects of several UAS components and operational parameters on material distribution were investigated. Specifically, the effect of (1) application height and spinner-disc speed, (2) different metering opening sizes (medium and large), and (3) the vane shape (curved and straight) on the distribution uniformity of cereal rye applied with a UAS was evaluated.

4.3 Materials and Methods

A commercially available UAS, the DJI Agras T25 (SZ DJI Technology Co., Shenzhen, China), was used for all experiments in this study [Figure 4.3(a)]. The DJI T25 features a quadcopter arrangement and a 35 L dry material tank capacity. A hopper (metering) gate [Figure 4.3(b & c)] with three equally sized slots regulates the amount of material flow onto a single broadcast disc. The manufacturer offers three hopper gate options (small, medium, and large) to meter material based on particle size and application rate. A single disc with eight curved vanes is installed directly below the hopper gate and broadcasts the product across the application swath. The DJI Agras App flight program, pre-installed on a DJI RC Plus remote controller, was used to operate the UAS and program its flight paths. During all field tests in this study, the T25 was connected to the Alabama CORS network to utilize RTK positioning, which provided horizontal and vertical position accuracy of ±10 cm. The detailed specifications for the DJI Agras T25 UAS are provided in Table 4.1. Cereal rye (*Secale cereale*) was used as the cover crop seed to be dispensed with the T25 and was acquired in the Fall of 2024. The bulk and particle density for the cereal rye used in this study were determined to be 68.2 kg m^{-3} and 1.2 g/cm^{-3}, respectively.

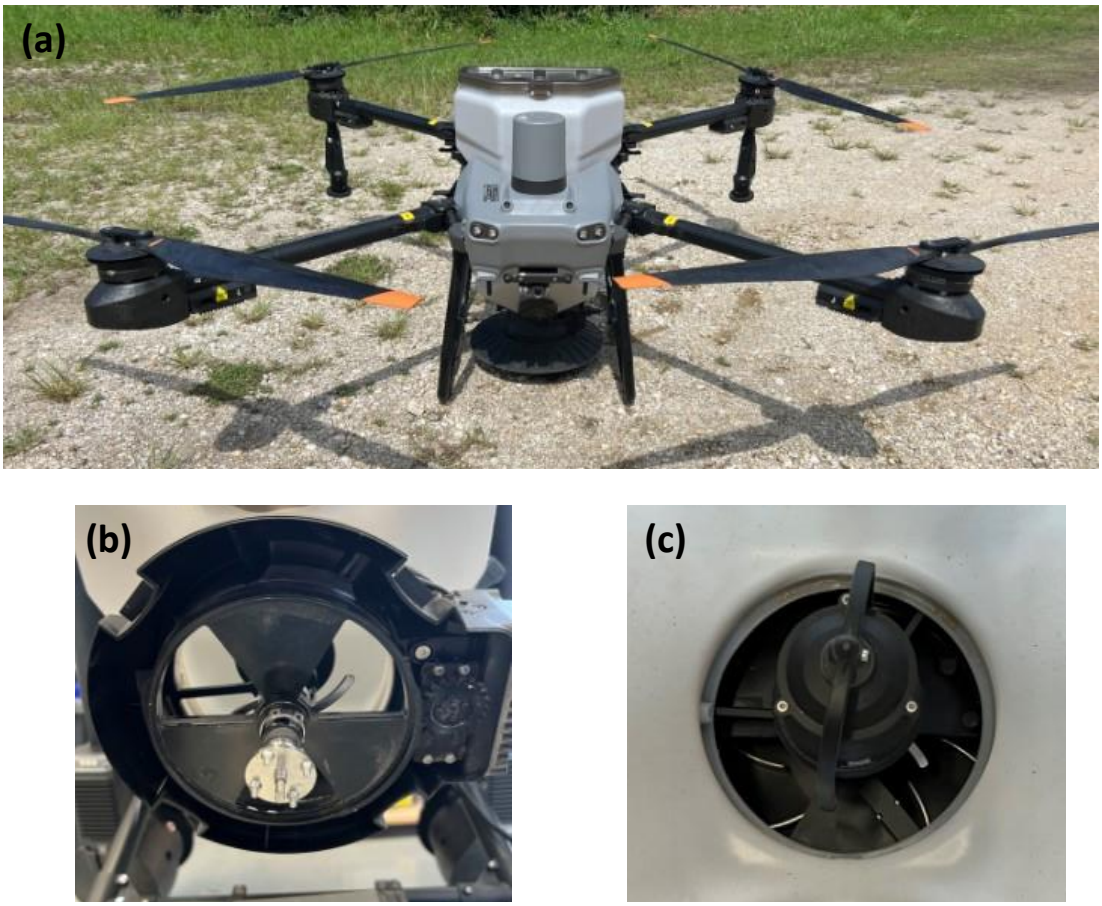

Figure 4.1. (a) DJI Agras T25 UAS used for the spreader performance studies, (b) metering gate and metering mechanism beneath the hopper, and (c) hopper (metering) gate as viewed through the empty hopper.

Table 4.2. Specifications for the DJI Agras T25 UAS.

Platform Weight (empty) (kg)	32
Payload (kg)	25
Dimensions (unfolded) (mm)	2585 × 2675 × 780
Tank Volume (L)	35
Hovering Time (full) (min)	6
Recommended Spreading Width (m)	5 – 8
Maximum Spreading Speed (m s^{-1})	10.0
Battery Capacity (mAh)	15,500

4.4 Experimental Design and Test Parameters

All field tests were conducted at the E.V. Smith Research Center in Shorter, AL (32°26'39.5" N 85°53'45.5" W) on a flat, open, and uncropped site in the Spring of 2025. The application area selected in the field for these tests was approximately 130 m long and 25.3 m wide. The DJI flight-planning software, DJI Agras App, was used to program a test flight consisting of a single pass of the UAS directly through the center of the application area. This flight plan was used throughout testing to ensure a consistent flight path across all study treatments. The field tests were conducted with the UAS in an autonomous mode, and different application parameters were entered in the remote controller prior to each flight. This study consisted of three field tests, each focused on assessing the effects of various operational or structural (design of metering and spreading components) parameters on the distribution uniformity of cereal rye within the swath. The first experiment was a factorial arrangement of application height and spinner-disc speed, with three UAS heights (3.0, 3.8, and 4.6 m) and three spinner-disc speeds (700, 1000, and 1300 RPM). The second experiment compared two hopper metering gate designs (medium and large) across application rates of 22.4, 33.6, and 44.8 kg ha^{-1}. These metering gates differed in the size and shape of the openings through which the material is dispensed from the hopper (Figure 4.2). The manufacturer recommends using the medium hopper gate [Figure 4.2(a)] for smaller materials or lower flow rates, while the larger gate [Figure 4.2(b)] is recommended for large granular materials and/or higher flow rates. While both hopper gates are suitable for spreading cereal rye, differences in hopper openings result in material being delivered to different locations on the spinner disk, thereby influencing material distribution. The third and final experiment investigated the effect of spinner-disc design [straight and curved vanes; Figures 4.2(c) & 4.2(d), respectively] on material distribution across application rates of 33.6, 44.8, and 56.0 kg ha^{-1}. The latest UAS models from

this manufacturer, such as DJI Agras T25 and T50, are equipped with a spinner-disc with curved vanes [Figure 4.2(c)], whereas a spinner-disc with straight vanes [Figure 4.2(d)] was common on the previous UAS models, such as the DJI Agras T30 and T40. Both spinner-disc designs are currently being used by UAS applicators for cover crop applications. Both spinner discs have a similar (4-hole) mounting pattern and thus can be easily swapped on the dry spreader system. The application parameters for each field test are provided in Table 4.2. During all experiments, each single pass of the UAS represented a combination of the application parameters being tested, with each test replicated four times. Across all experiments, a fixed UAS speed of 10 m s^{-1} was used.

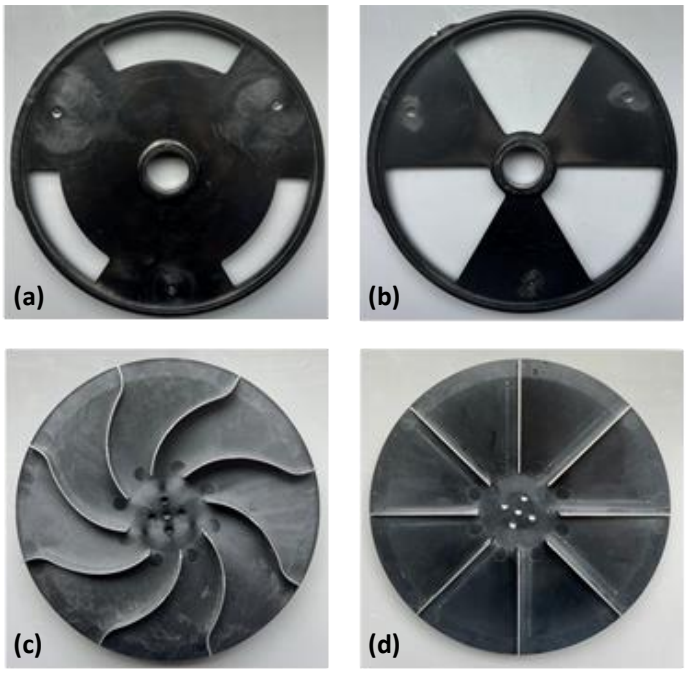

Figure 4.2. a) Medium hopper gate, b) large hopper gate, c) curved-vane spinner-disc and d) straight-vane spinner disc, used during the field testing.

Table 4.2. Information on different application parameters and their levels used during the field tests.

Field Test	Parameters Tested	Metering Gate	Spinner Disc	Rate (kg ha^{-1})	Height (m)	Spinner Speed (RPM)
1	Application Height and Spinner	Large	Curved	44.8	3.0	700
				44.8	3.8	700
				44.8	4.6	700

	Speed	Large	Curved	44.8	3.0	1000
				44.8	3.8	1000
				44.8	4.6	1000
		Large	Curved	44.8	3.0	1300
				44.8	3.8	1300
				44.8	4.6	1300
2	Hopper Metering Gate	Medium	Curved	22.4	3.8	1000
				33.6	3.8	1000
				44.8	3.8	1000
		Large	Curved	22.4	3.8	1000
				33.6	3.8	1000
				44.8	3.8	1000
3	Spreading Disc with Straight and Curved Vanes	Large	Curved	33.6	3.8	1000
				44.8	3.8	1000
				56.0	3.8	1000
		Large	Straight	33.6	3.8	1000
				44.8	3.8	1000
				56.0	3.8	1000

4.5 Pan Testing and Data Collection

To evaluate the spread uniformity of cereal rye across various field experiments, pan tests were conducted in accordance with the procedures outlined in ASBAE Standard S386.2 (ASABE, 2018). Collection pans measuring 50.0 cm × 50.0 cm × 8.9 cm [Figure 4.4(a)] were used to collect the cereal rye broadcast by the UAS. These pans met the collector size requirements specified in ASBAE S386.2 and the ISO 5690-2:1984 standards (ISO, 2021). A total of 27 pans, spaced at 0.91 m intervals from center to center, were arranged in a single line within the application area, as shown in Figure 4.4(b). Within each pan, a set of baffles was placed to reduce the material bouncing out of the pans and improve collector efficiency [Figure 4.4(a)]. The collection line (consisting of evenly spaced pans) was arranged perpendicular to the UAS flight path and centered directly within it. The total distance covered by the pans was 24.6 m, more than three times the maximum spread swath (7-8 m) recommended by the manufacturer.

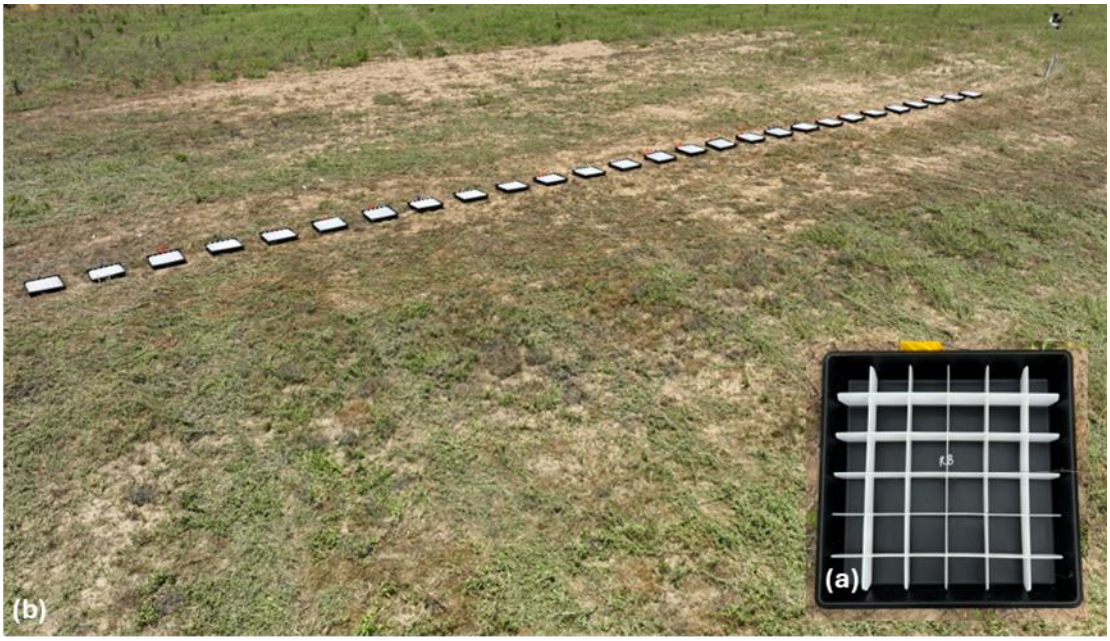

Figure 4.3. a) Collection pan used for UAS spreading data collection, and (b) experimental layout with collection pans placed within the application area.

During each test, the UAS performed a single pass over the collection pans with the desired application parameters (specific to the field test being conducted) preset in the controller and broadcast the material within the application area. After each flight, the material from each pan was carefully collected in a small, pre-labeled bag and stored for later weighing. During all field tests, a weather station (Vantage Pro2, Davis Instruments, Hayward, CA) was installed to record meteorological conditions, including wind speed and direction, temperature, and relative humidity, in 1.0-minute intervals. The station was installed at a height of 1.8 m above ground and was located approximately 10.0 m away from the outermost collection pan on one side of the swath. The meteorological data averaged for the duration of each field test is presented in Table 4.3. Weather conditions remained consistent throughout the field tests, in accordance with ASABE S386.2, with wind speed remaining low (<1.9 m s-1) during all three tests. The wind direction was north-northeast and remained within ±15° of the collection pans' orientation throughout the testing.

Table 4.3. Meteorological conditions recorded during different field tests conducted for assessing UAS application performance. Values are reported as mean ± standard deviation.

Field Test	Wind Speed[a] ($m\ s^{-1}$)	Temperature[a] (˚C)	Relative Humidity[a] (%)
1	1.1 ± 0.4	30.2 ± 0.1	50.6 ± 1.0
2	0.5 ± 0.4	24.2 ± 0.3	74.4 ± 0.8
3	1.2 ± 0.4	23.2 ± 0.3	77.5 ± 1.5

[a] Values represent mean ± standard deviation.

4.6 Data Analysis

The cereal rye collected in the pans during the field tests was weighed using a scale with a readability of 0.01g (Ohaus Scout SPX222, Ohaus Corporation, Parsippany, New Jersey) and recorded in an MS Excel sheet. Then, the weight in each pan was converted to an applied rate in kilograms per hectare using the pan opening area and a collector efficiency of 100%, per ASABE Standard S386.2 (ASABE, 2024). Single-pass distribution patterns were generated by plotting the calculated mean applied rate ($kg\ ha^{-1}$) versus the transverse location of each pan within the swath. To develop simulated overlap patterns, which characterize the uniformity of distribution within the effective swath, an effective swath of 7.3 meters was generated for each test treatment using a progressive application method, as defined in the ASABE S386.2. For all simulated patterns across different treatments, the mean applied rate and coefficient of variation (CV), which represents the distribution uniformity within the swath, were computed using equations in ASABE S386.2. For a separate comparison to the progressive application method, simulated overlap patterns were generated for the one-direction method using the single pass data from each test. Each data set from the field tests were subjected to ANOVA to determine the effects of the main treatments and their interaction on the spreading distribution. All statistical analyses were conducted at $\alpha = 0.05$, while means for significant effects were separated using the Student's t-test ($p \leq 0.05$).

4.7 Results and Discussion

4.7.1 Effect of Application Height and Spinner-Disc Speed

The graphs in Figure 4.4 depict the single-pass and overlap spread patterns for cereal rye applied with the UAS at different application heights (a and c, respectively) and spinner-disc speeds (b and d, respectively). The single-pass patterns showed a leftward skewness, with a peak indicating greater cereal rye deposition between 0 and -2 m within the swath. This leftward skew is typical of single-disc broadcast systems and has also been reported by other researchers (Han et al., 2015; Sizemore et al., 2026). Statistical analysis indicated no significant interaction between application height and spinner-disc; hence, the summary statistics for their effects on material distribution are presented separately in Table 4.4. A visual comparison of the single-pass spread patterns across different application heights suggests greater material deposition, especially towards the middle of the swath (-2 to 2 m), as application height decreased. Statistically, the total amount of material deposited within the swath was also lower at the application height of 4.6 m than at the heights of 3.0 and 3.8 m (Table 4.4). A similar effect of spinner-disc speed was observed, with applications at 1000 and 1300 rpm exhibiting greater cereal rye deposition within the swath than at 700 rpm. A plausible explanation of why the amount of material decreased in these two instances is due to the dry material velocity as it falls from the spinner disc spreader. The cereal rye was allowed a longer duration to fall toward the collectors, and as such, gained greater velocity and impact force on the collectors, especially for the test involving application height. For the field test involving different spinner disc speeds, the reduced horizontal force exerted on the cereal rye (as evidenced by the reduced swath width) likely led to more vertical seed trajectory into the collectors rather than more horizontal entrance angles. In both cases, the seed impact with the collector likely led to a greater rebound force of the cereal seed up and out of the collectors.

For maximum single-pass swath, an increase in both application height and spinner-disc speed resulted in an increased swath (Table 4.4), with more material reaching farther towards the left side of the swath. This can also be observed in single-pass patterns in Figure 4.4(a) and 4.4(b) for the effect of application height and spinner-disc speed, respectively. These results were consistent with those of Song et al. (2023), showing increased effective swath widths at higher application heights when flight speed was held constant. For spread pattern skewness, there was no effect of application height or spinner-disc speed, with similar amounts of cereal rye deposition towards the left (49 – 53%) and right (38 – 40%) sides of the swath across different heights and speeds.

Consequently, an analysis of the overlap spread patterns indicated similar mean applied rates (47.9 to 54.6 kg ha^{-1}) across different application heights and spinner-disc speeds tested in this study (Table 4.4). The cereal rye distribution across the swath was also similar across different application heights (CV = 30–33%), indicating no significant effect of height on spread uniformity. In contrast, the spinner-disc speed affected distribution uniformity, with greater variability in cereal rye distribution at 700 rpm (CV = 38%) than at 1000 or 1300 rpm (CV = 26–31%). The overlap spread patterns in Figure 4.4(d) verify these findings, where the cereal rye deposition within the swath is more uniform (and comparable) at spinner-disc speeds of 1000 and 1300 rpm than at 700 rpm. Thomas (2025) performed a similar test with a DJI Agras T20P spreader and evaluated different spinner-disc speeds of 550, 800, 1050, and 1300 rpm. The author reported the highest skewness in the spread pattern and a narrower swath at the lowest speed of 550 rpm; however, the effects of other spinner-disc speeds were not significantly different, producing similar swaths and material distribution within the swath.

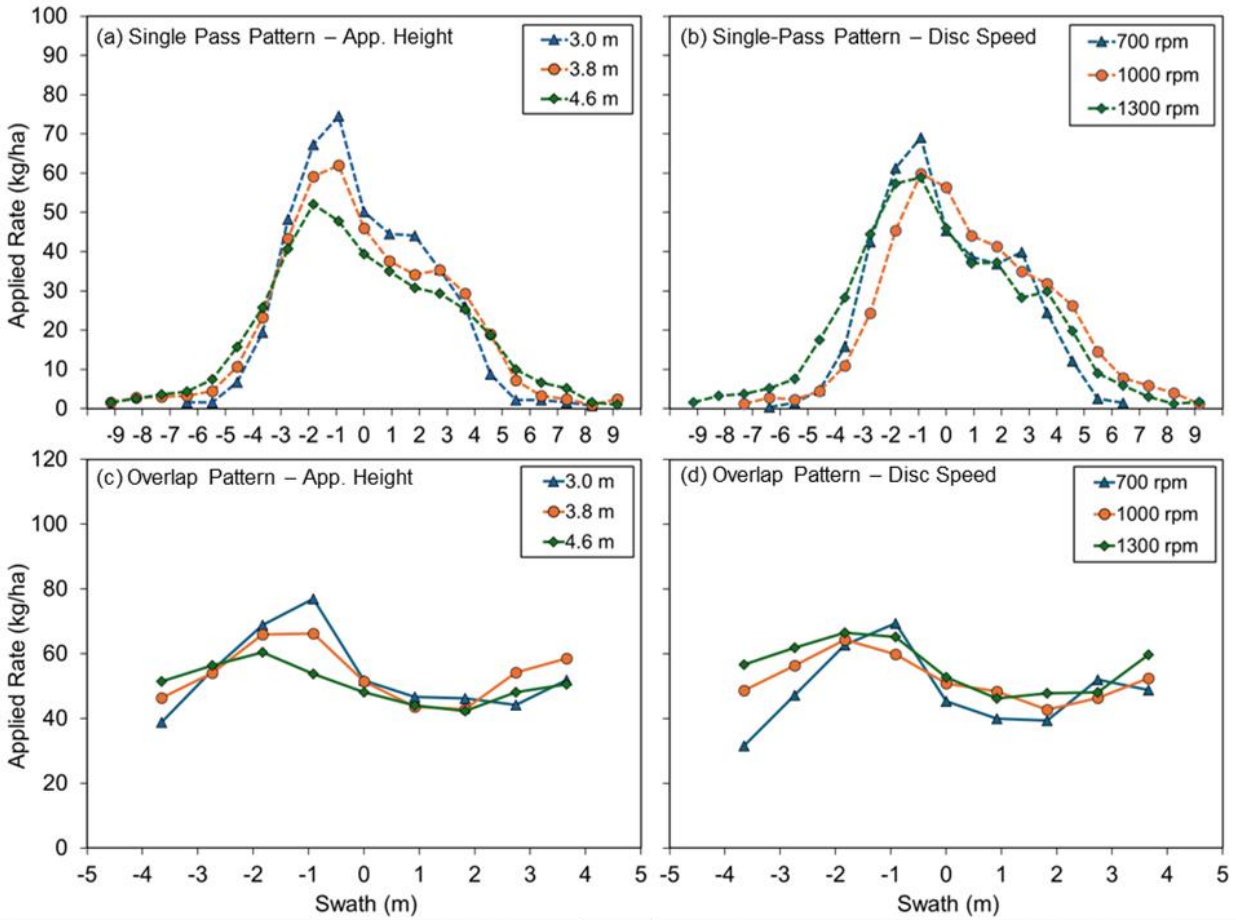

Figure 4.4. Single-pass (a & b) and simulated overlap (c & d) spread patterns representing cereal rye application with a UAS at different application heights and spinner-disc speeds, respectively, at a target application rate of 44 kg ha^{-1}. 0 m on the graphs coincides with the center of the UAS flight path (swath).

Table 4.4. Summary Statistics for the single-pass and simulated overlap spread patterns for cereal rye applied with the UAS at different application heights and spinner-disc speeds.

Test Parameter	Level	Single-Pass Spread Pattern[a]			Overlap Spread Pattern[a]	
		Total Mass (kg x 10^{-3})	Maximum Swath (m)	Skewness % (L/R)	Mean Rate (kg ha^{-1})	CV (%)
Application Height (m)	3.0	10.6 a	11.0 c	50/38	52.3	33
	3.8	10.2 a	12.5 b	49/40	51.6	30
	4.6	9.7 b	13.4 a	53/40	49.4	31
Spinner Disc Speed (RPM)	700	9.7 B	10.2 C	49/39	47.9	38 A
	1000	10.0 A	12.2 B	53/39	50.8	31 B
	1300	10.8 A	14.5 A	50/40	54.6	26 B

[a] Values followed by the same letters within each column are not significantly different from each other ($p>0.05$).

4.7.2 Effect of Hopper (metering) Gate Design (Opening Size)

The effects of hopper gate design (opening size) were similar across the application rates tested in this study and was determined to have no interaction; hence, the spread patterns (Figure 4.5) and summary statistics (Table 4.5) are presented separately for these parameters. While small differences in single-pass patterns between the medium and large metering gates can be observed in Figure 4.5(a), the total material (by mass) collected across the swath was similar across both gates (Table 4.5). As expected, the total material within the swath increased with application rate because more material was metered through both gates, as observed in Figure 4.5(b). The effect of metering gate design was observed in the maximum single-pass swath, with the medium gate exhibiting a wider swath (by 1 m) than the large gate. This can be attributed to the difference in the drop location of cereal rye on the spinner-disc between the two gates. The design of the openings on the medium hopper gate is such that the material drops towards the outer edge of the spinner-disc [Figure 4.2(a)], thereby travelling farther within the swath. For the large gate, the openings are designed such [Figure 4.2(b)] that the material drops mostly equally from the center towards the outward edge of the spinner-disc. While the maximum single-pass swath increased slightly with increasing application rate, it was not statistically different across rates. Similarly, there was no effect of metering gate or application rate on the spread pattern skewness, with approximately 54% to 59% of the cereal rye deposited towards the left side of the swath and 31% to 35% of cereal rye deposited to the right side across the two hopper gates and different application rates.

While the overlap patterns show slight differences between the two metering gates [Figure 4.5(c)], the mean applied rate and distribution uniformity were comparable, indicating no significant effect of gate design (opening size) on the applied rate or the spreading distribution of

cereal rye within the swath. Again, as expected, the mean applied rate increased with the application rate (Table 4.5), as evidenced by the change in the magnitude of the overlap patterns in Figure 4.5(d). However, the distribution of cereal rye was statistically similar across the different rates (CV = 33 – 42%), suggesting similar spread uniformity with increasing application rate. Parish and Chaney (1986) determined that adjusting the drop point location can improve material skewness to some extent, though it will not fully overcome all distribution challenges (i.e., inherent skewness with single-disc designs). Grift and Kweon (2006) conducted similar testing, combining both lab and simulated trials. The results were comparable, with a rotation in the drop point around the spinner disc resulting in improved CV values for simulated overlap passes.

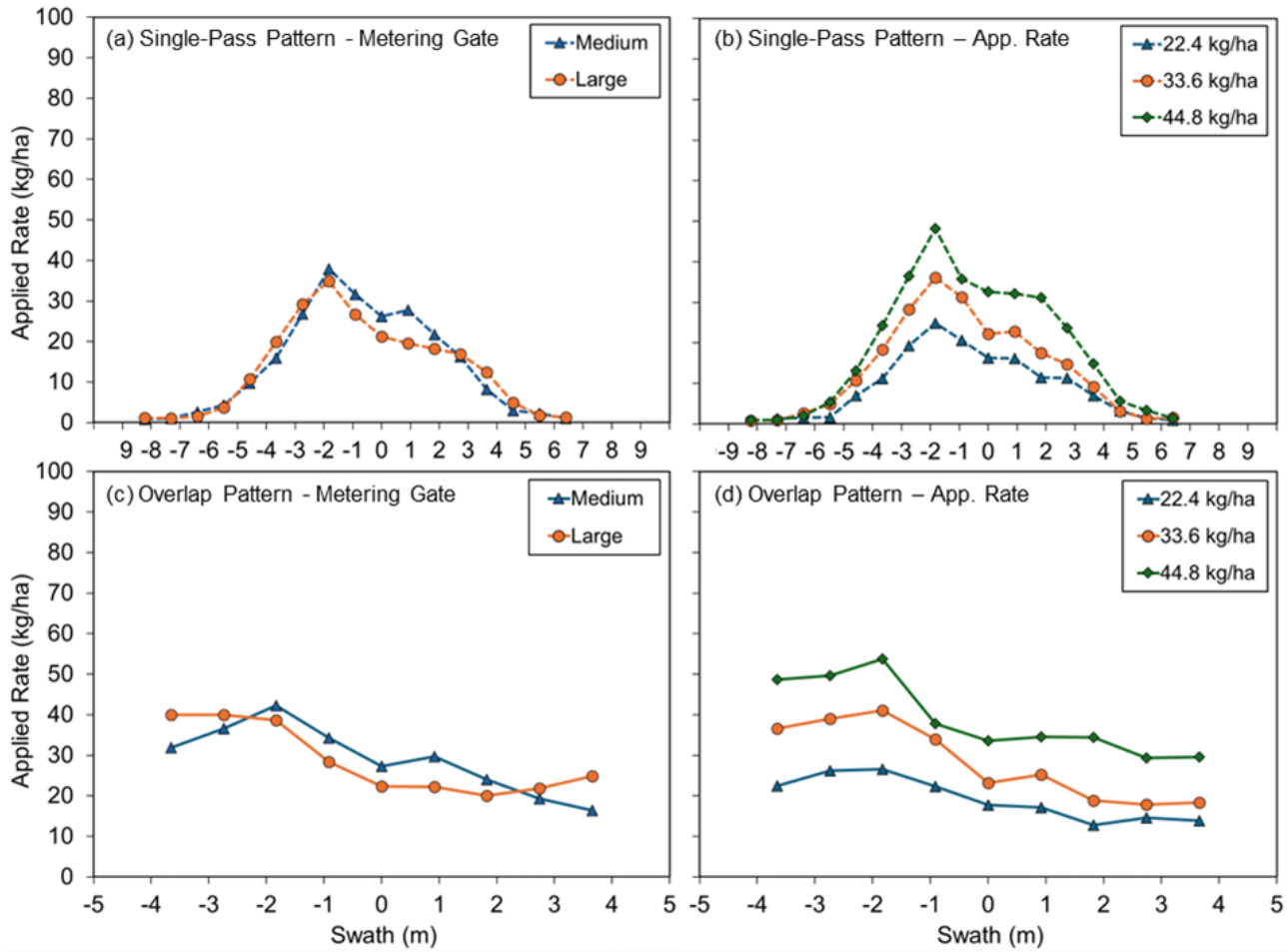

Figure 4.5. Single-pass (a & b) and simulated overlap (c & d) spread patterns representing cereal rye application with a UAS with different metering gates and application rates tested across each gate, respectively. 0 m on the graphs coincides with the center of the UAS flight path (swath).

Table 4.5. Summary Statistics for the single-pass and simulated overlap spread patterns for cereal rye application with the UAS using different metering gates and application rates tested across both gates.

Test Parameter	Level	Single-Pass Spread Pattern[a]			Overlap Spread Pattern[a]	
		Total Mass (kg x 10^{-3})	Maximum Swath (m)	Skewness % (L/R)	Mean Rate (kg ha^{-1})	CV (%)
Metering Gate	Medium	5.8	12.9 a	56/33	28.8	37
	Large	5.6	11.9 b	57/33	28.7	37
Application Rate	22.4	3.8 C	12.0	56/33	19.0 C	36
	33.6	5.5 B	12.3	59/31	27.9 B	42
	44.8	7.9 A	12.8	54/35	39.4 A	33

[a] Values followed by the same letters within each column and for each main effect are not significantly different from each other ($p>0.05$).

4.7.3 Effect of Spreading Disc Design (Vane Shape)

Similar to the hopper gate design, the effect of spinner-disc design did not have any interaction with the tested application rates. The data is presented for each main effect in Figure 4.6 and Table 4.6. The single-pass spread pattern for the spinner-disc with curved vanes had a slightly higher peak and was shifted towards the left of the swath as compared to the spread pattern for the straight-vane spinner-disc. The skewness data also confirmed these visual differences, with 57% of the cereal rye deposition towards the left of the swath for the curved-vane spinner-disc, compared to 51% for the spinner-disc with straight vanes (Table 4.6). The total material deposited within the swath and the maximum single-pass swath were also greater (by 0.6×10^{-3} kg and 1.1 m, respectively) for the curved-vane design than for the straight-vane disc. The application rate showed a similar effect across both disc types, as noticed in the previous tests, where the total mass deposited within the swath increased with rate, but the maximum swath (12.0 – 12.9 m) and the pattern skewness were statistically similar across the application rates. For overlap patterns, the mean applied rate was significantly greater for the spinner-disc with curved vanes than for the

straight-vane disc (Table 4.6). Though some visual differences can be observed among the overlap patterns for the straight-vane and curved-vane disc designs [Figure 4.6(c)], the CV values were comparable across both spinner-disc types (29 – 34%), indicating no significant effect of spinner-disc design or vane shape on the spread uniformity of cereal rye applied with the UAS.

For the application rate, the mean applied rate increased with the target rate, while the distribution uniformity of cereal rye was similar across rates, with CV values ranging from 30% to 34%. Yilidiran & Kara (2012) determined that a fertilizer spreader disc with only straight vanes did not provide ideal uniformity within the spread swath, but rather a disc with a combination of both curved and straight vanes offered the best uniformity. Yilidiran (2008) tested the effect of the number of vanes on a rotary disc and found that spreading uniformity deteriorated as the number of vanes increased. Xunwei et al. (2024) conducted simulated distribution uniformity testing utilizing field data collected from a DJI Agras T60. The authors tested straight and curved vanes with different deflection angles and reported that, as spread uniformity generally improved with deflection angle, the straight vanes were a critical design feature that complemented the curved vanes. They also found that the increased deflection angle began to cause the fertilizer to stick within the curves and not release through centrifugal force. Future research should investigate the effects of vane number or a combination of straight and curved vanes on the uniformity of material distribution when applied with single-disc UAS spreaders.

Overall, these findings in the present study suggested that the spinner-disc with curved vanes demonstrated improved spreading performance with a wider single-pass swath and increased material deposition within the swath. This could also explain the transition by manufacturers, especially DJI, toward curved-vane designs on newer UAS models, compared to the prevalent straight-vane disc designs on previous models.

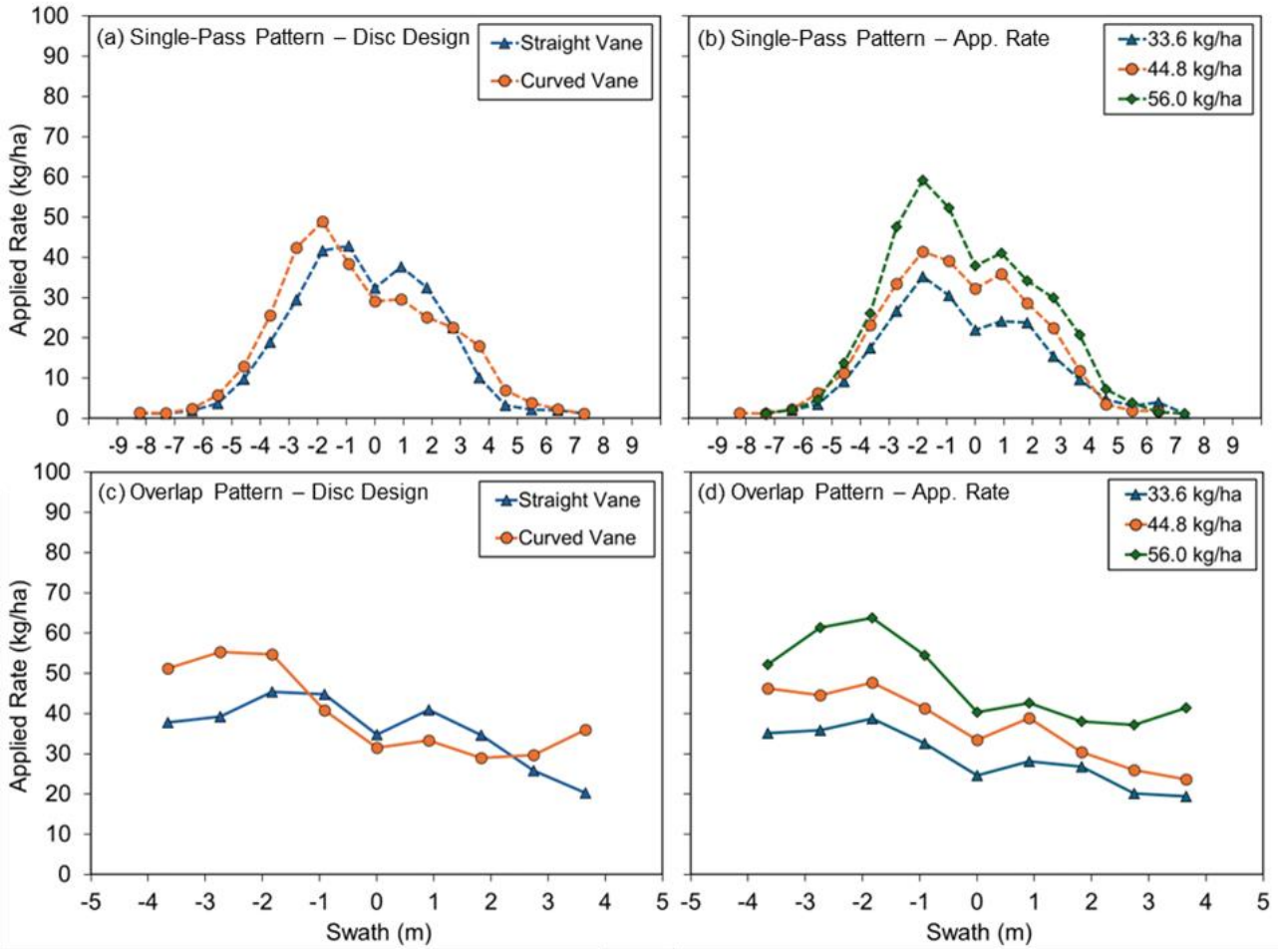

Figure 4.6. Single-pass (a & b) and simulated overlap (c & d) spread patterns representing cereal rye application with a UAS with different spreading disc designs and application rates tested across each disc, respectively. 0 m on the graphs coincides with the center of the UAS flight path (swath).

Table 4.6. Summary Statistics for the single-pass and simulated overlap spread patterns for cereal rye application with the UAS using spreading discs with different vane designs and application rates tested across each disc.

Test Parameter	Level	Single-Pass Spread Pattern[a]			Overlap Spread Pattern[a]	
		Total Mass (kg x 10^{-3})	Maximum Swath (m)	Skewness % (L/R)	Mean Rate (kg ha^{-1})	CV (%)
Spinner Disc Design	Straight	7.2 b	11.9 b	51/37 a	35.3 b	29
	Curved	7.8 a	13.0 a	57/34 b	39.5 a	34
Application Rate	33.6	5.6 C	12.0	55/36	28.2 C	32
	44.8	7.3 B	12.5	53/36	36.5 B	34
	56.0	9.5 A	12.9	54/36	47.6 A	30

[a] Values followed by the same letters within each column and for each main effect are not significantly different from each other ($p>0.05$).

4.7.4 Comparison of Application Methods – Progressive versus One-Direction

The simulated overlap patterns (for an effective swath of 7.3 m) were also generated using the one-direction (ASABE Standards, 2024) method to determine whether the application pattern has any effect on the spreading uniformity of cereal rye within the swath. The progressive method method uses a progressive application pattern, with the UAS direction of travel changing from pass to pass. This produces a spread pattern with right-on-right and left-on-left wing overlap. In contrast, the one-direction (also known as racetrack) method is characterized by the same travel direction from pass to pass and results in a right-on-left and left-on-right wing spread pattern. Statistical analysis suggested that the effect of the application method was consistent across different levels of operational parameters tested within each field test; hence, the results summarizing the differences between the two application methods are presented by field test (Table 4.7).

Across all three field tests, the one-direction pattern exhibited CV values 6% to 12% lower than those of the progressive application pattern, suggesting improved cereal rye distribution within the swath when applied with the UAS using the one-direction method. These results were similar to those attained by Sizemore et al. (2026), where the one-direction method demonstrated 5% to 7% lower CV values than for the progressive method for experiments involving the application of cereal rye with the same UAS (DJI T25) at various target rates and flight speeds. In addition to optimizing operational parameters, adjusting application patterns, such as using a one-direction method, could be another effective strategy for UAS operators to improve the application uniformity of cereal rye and other cover crop seed.

Table 4.7. Comparison of the distribution uniformity (CV) of cereal rye application with a UAS between the progressive and one-direction application methods.

Field Test	Test Parameters	Application Method	CV[a] (%)
1	Application Height × Disc Speed	Progressive	32 a
		One-Direction	26 b
2	Metering Gate × Application Rate	Progressive	37 a
		One-Direction	25 b
3	Spinner Disc Design × Application Rate	Progressive	32 a
		One-Direction	23 b

[a] Values followed by the same letters within each column are not significantly different from each other ($p>0.05$).

4.8 Conclusions

Field experiments were conducted to determine the effect of different operational (application height and spinner-disc speed) and structural parameters (metering gate and spinner-disc design) on the spreading distribution of cereal rye applied with a commercial UAS (DJI Agras T25). Single-pass spread patterns showed a leftward skewness – typical of single-disc broadcast spreaders – with heavy material deposition towards the left of the swath. Both application height & spinner-disc speed affected the total material deposited within the swath and the maximum single-pass swath, while the spread pattern skewness was similar across different heights and disc speeds. The maximum single-pass swath increased with an increase in application height and spinner-disc speed, with swath ranging from 11.0 to 13.4 m across the heights and from 10.2 to 14.5 m across the spinner-disc speeds. Despite differences in total material deposited in single-pass, the mean applied rate for the simulated overlap pattern (effective swath = 7.3 m) was similar across the application heights and between the spinner-disc speeds. The distribution uniformity of cereal rye was not affected by application height, but the lower spinner-disc speed of 700 rpm exhibited greater in-swath variability than the 1000 and 1300 rpm speeds. For the metering gate design, the medium gate provided a wider swath than the large gate; however, the spread pattern skewness for single-pass, and the mean applied rate and distribution uniformity for the simulated

overlap pattern were statistically similar across both gates. A comparison of the straight and curved spinner-discs showed greater material deposition, wider swath, and higher skewness in the single-pass patterns for the curved design than the spinner-disc with straight vanes. The curved-vane disc also exhibited a higher mean applied rate for the simulated overlap pattern, but no improvement in spreading uniformity over the straight-vane disc. A uniformity analysis by application method also suggested improved CV values for the one-direction application method compared to the progressive application pattern, commonly used by most of the latest UAS models. Future studies should investigate the application performance of newer auger-type metering systems, as well as the effects of other spinner-disc designs, including vane shape and number, on spreading distribution.

Chapter Five

Conclusions

The use of unmanned aerial systems (UAS) for applying dry solid materials, especially cover crop seed, has grown rapidly in recent years within the United States. Due to the limited research on dry spreading systems on UAS, studies were conducted to evaluate their application performance, in terms of metering accuracy and distribution uniformity across the swath, as well as to investigate the effects of various operational and structural parameters on spreading performance. Cereal rye was used as a cover crop seed in these studies due to its widespread use.

In the first study, the accuracy of the manufacturer's internal calibration process and the applied rate accuracy of a commercially available UAS (DJI Agras T25) was evaluated through static and field testing across varying application rates (22.4, 33.6, 44.8, 56.0 and 64.3 kg ha^{-1}) and flight speeds (6, 7, 8, 9, & 10 m s^{-1}). Calibration results showed that the actual material flow rate differed considerably from the rate suggested by the manufacturer's calibration procedure, resulting in under-application ranging from 9.5% to 17.7% during field tests of cereal rye applied with the UAS at different target rates and flight speeds. The highest under-application occurred at the target rate of 22.4 kg ha^{-1} and flight speed of 6 m s^{-1}, corresponding to metering gate openings ≤30%. These metering issues at lower gate openings were due to bridging of cereal rye seed, underscoring the importance of proper metering gate selection based on target application rate and the type of material being spread. The second objective of this study was to determine the spread distribution and uniformity across the swath at the aforementioned application rates and flight speeds. The single-pass distribution patterns for cereal rye exhibited leftward skewness, with a maximum swath width ranging from 11.9 to 13.6 m across different tested parameters. The effect of application rate and flight speed on spread pattern skewness varied among the rates and speeds.

While the total material deposited within the single-pass swath increased with application rate, it was similar across different flight speeds, indicating no adverse effect on material deposition at higher flight speeds. The simulated overlap patterns (for an effective swath of 7.3 m) exhibited variable distribution uniformity, with CV values ranging from 19% to 39%, regardless of the rate and speed. The mean applied rate within the simulated overlap pattern increased with the target rate but remained comparable across the flight speeds. A comparison of application methods demonstrated improved cereal rye deposition uniformity for the one-direction application method compared to the progressive application pattern. An analysis of spread uniformity at different effective swaths did not show improved distribution uniformity for applications at narrower swaths (<5 m) compared to the nominal wider swaths used by UAS operators (5 – 7 m).

The second study evaluated the effect of various operational parameters, such as application speed and spinner-disc speed, on material distribution within the swath. The first objective of this study was to evaluate single-pass and overlap spread patterns at varying application heights of 3.0, 3.8, and 4.6 m, and spinner disc speeds of 700, 1000, and 1300 RPM for cereal rye applied with a UAS (DJI Agras T25). Results showed that both application height and spinner-disc speed affected cereal rye distribution within the swath, with single-pass spread patterns showing lower material deposition at an application height of 4.6 m and a spinner-disc speed of 700 rpm compared to other heights and speeds. Similarly, the maximum single-pass swath increased from 11.0 to 13.4 m with an increase in application height, and from 10.2 to 14.5 m with an increase in spinner-disc speed. The overlap spread patterns indicated similar mean applied rates and spreading distribution (CV = 30–33%) across different application heights and spinner-disc speeds. However, the distribution uniformity of cereal rye was better at the spinner-disc speeds of 1000 and 1300 rpm (CV = 26–31%) than at 700 rpm (CV = 38%). Another objective of this study was to evaluate the effect of

metering gate design (medium and large gates with varied opening sizes) on the spread distribution of cereal rye across varying application rates (22.4, 33.6 and 44.8 kg ha^{-1}). The medium gate exhibited a wider maximum single-pass swath than the large gate, but there were no differences in total material deposited within the swath and skewness for single-pass spread patterns. Similarly, the mean applied rate and distribution uniformity were similar across both metering gate designs. The final objective of this study investigated two spinner-disc designs (straight vane and curved vane) and their effect on material distribution was tested across different application rates (33.6, 44.8 and 56.0 kg ha^{-1}). The curved-vane disc (13.0 m) exhibited a wider single-pass swath compared to the curved-vane disc (11.9 m) and also resulted in spread patterns with greater leftward skewness. The curved-vane design also exhibited a higher mean applied rate, but the distribution uniformity of overlap spread patterns was comparable (CV values between 29% and 34%) between the two spinner-disc types.

The findings of these two studies provide insight into how certain operational parameters affect the distribution uniformity of cereal rye within the swath. UAS platforms have numerous advantages over traditional cover crop seeding methods, but they do require accurate calibration and appropriate parameter selection for optimal application quality, just as traditional methods do. Though there are numerous UAS models that use similar design features to those detailed in these studies, other models, such as newer DJI or XAG offerings, use different metering systems and spreading methods. These newer metering and spreading systems should be evaluated in future studies, as they are becoming increasingly popular on the latest UAS models. Furthermore, investigations into seeding various cover crop mixtures with UAS should be undertaken, as these materials vary in physical properties and are likely to exhibit differences in spread patterns and distribution uniformity than those obtained in the current studies. The information gained in these

studies is valuable for improving the application of dry materials and advancing the development of dry spreading systems and technology for effective applications with UAS.

References

Ahmad, F., Qiu, B., Dong, X., Ma, J., Huang, X., Ahmed, S., & Ali Chandio, F. (2020). Effect of operational parameters of UAV sprayer on spray deposition pattern in target and off-target zones during outer field weed control application. *Computers and Electronics in Agriculture*, *172*, 105350. https://doi.org/10.1016/j.compag.2020.105350

American Spray Drone Coalition. (2024). *Impact Of Spray Drones In Agriculture*. ASDC. https://americanspraydronecoalition.com/wp-content/uploads/2025/02/Impact-of-Drones-in-Agriculture-Infographic.pdf

ASABE Standards. (2024). S386.2: Calibration and distribution pattern testing of agricultural aerial application equipment. St. Joseph, MI: ASABE.

Barbosa Júnior, M. R., Moreira, B. R. D. A., Carreira, V. D. S., Brito Filho, A. L. D., Trentin, C., Souza, F. L. P. D., Tedesco, D., Setiyono, T., Flores, J. P., Ampatzidis, Y., Silva, R. P. D., & Shiratsuchi, L. S. (2024). Precision agriculture in the United States: A comprehensive meta-review inspiring further research, innovation, and adoption. *Computers and Electronics in Agriculture*, *221*, 108993. https://doi.org/10.1016/j.compag.2024.108993

Barnes, J. P., & Putnam, A. R. (1983). Rye residues contribute weed suppression in no-tillage cropping systems. *Journal of Chemical Ecology*, *9*(8), 1045–1057. https://doi.org/10.1007/BF00982210

Basche, A. D., Kaspar, T. C., Archontoulis, S. V., Jaynes, D. B., Sauer, T. J., Parkin, T. B., & Miguez, F. E. (2016). Soil water improvements with the long-term use of a winter rye cover crop. *Agricultural Water Management*, *172*, 40–50. https://doi.org/10.1016/j.agwat.2016.04.006

Bergtold, J. S., Ramsey, S., Maddy, L., & Williams, J. R. (2019). A review of economic considerations for cover crops as a conservation practice. *Renewable Agriculture and Food Systems*, *34*(1), 62–76. https://doi.org/10.1017/S1742170517000278

Bird, S. L., Esterly, D. M., & Perry, S. G. (1996). Off-Target Deposition of Pesticides from Agricultural Aerial Spray Applications. *Journal of Environmental Quality*, *25*(5), 1095–1104. https://doi.org/10.2134/jeq1996.00472425002500050024x

Bowman, M., & Morales, M. (20246). *2022 Census of Agriculture: Cover crop use continues to be most common in eastern United States*. Ers.Usda.Gov. https://www.ers.usda.gov/data-products/charts-of-note/chart-detail?chartId=108950

Byers, C., Virk, S., Rains, G., & Li, S. (2024). Spray deposition and uniformity assessment of unmanned aerial application systems (UAAS) at varying operational parameters. *Frontiers in Agronomy*, *6*, 1418623. https://doi.org/10.3389/fagro.2024.1418623

Dapaah, H. K., & Vyn, T. J. (1998). Nitrogen fertilization and cover crop effects on soil structural stability and corn performance. *Communications in Soil Science and Plant Analysis*, *29*(17–18), 2557–2569. https://doi.org/10.1080/00103629809370134

Floyd M. Cunningham. (1963). Performance Characteristics of Bulk Spreaders for Granular Fertilizer. *Transactions of the ASAE*, *6*(2), 0108–0114. https://doi.org/10.13031/2013.40839

Fulton, J. P., Thaper, R. K., Virk, S. S., McDonald, T., & Fasina, O. (2020). Effect of Vane Shape on Fertilizer Distribution for a Dual-Disc Spinner Spreader. *Applied Engineering in Agriculture*, *36*(5), 743–751. https://doi.org/10.13031/aea.13634

Gohari, A., Ahmad, A. B., Rabiu, L., Rahim, R. B. A., Supa'at, A. S. M., Elamin, N. I. M., Gismalla, M. S. M., Al-Dharrab, S. I., Rashid, R. A., Nawawi, S. W., Nasir, N., Sarijari, M. A. B., Darwin, N. B., & Muqaibel, A. H. (2024). A Systematic Review of the UAV Technology Usage in

ASEAN. *IEEE Open Journal of Vehicular Technology*, *5*, 1036–1058. https://doi.org/10.1109/OJVT.2024.3436065

Güneş, D., & Hasegawa, H. (2025). Optimizing UAV sprayer performance using field data and machine learning approaches. *Smart Agricultural Technology*, *11*, 101013. https://doi.org/10.1016/j.atech.2025.101013

Han, C., Lee, S., Hong, Y., Kweon, G. (2019). Development of a variable rate applicator for uniform fertilizer spreading. *International Journal of Agricultural and Biological Engineering*, *12*(2), 82–89. https://doi.org/10.25165/j.ijabe.20191202.3242

Han, C.-W., Park, H., Lee, S., Hong, Y., Lee, Hoon, & Kweon, G. (2015). Pattern Analysis of a Single-disc Granule Spreader for Uniform Application of Fertilizer. *Journal of Agriculture & Life Science*, *49*(5), 321–332. https://doi.org/10.14397/jals.2015.49.5.321

He, X. K., Bonds, J., Herbst, A., & Langenakens, J. (2017). Recent development of unmanned aerial vehicle for plant protection in East Asia. *International Journal of Agricultural and Biological Engineering*, *10*(3), 18–30. https://doi.org/10.3965/j.ijabe.20171003.3248

Hofstee, J. W. (1992). Handling and spreading of fertilizers: Part 2, physical properties of fertilizer, measuring methods and data. *Journal of Agricultural Engineering Research*, *53*, 141–162. https://doi.org/10.1016/0021-8634(92)80079-8

Hofstee, J. W., & Huisman, W. (1990). Handling and spreading of fertilizers part 1: Physical properties of fertilizer in relation to particle motion. *Journal of Agricultural Engineering Research*, *47*, 213–234. https://doi.org/10.1016/0021-8634(90)80043-T

Influence of Broiler Litter Bulk Density on Metering and Distribution for a Spinner-Disc Spreader. (2013). *Applied Engineering in Agriculture*. https://doi.org/10.13031/aea.29.9993

International Society of Precision Agriculture. (n.d.). *Definition of Precision Agriculture*. Retrieved October 19, 2025, from https://www.ispag.org/resources/definition

J. B. Davis & C. E. Rice. (1974). Predicting Fertilizer Distribution by a Centrifugal Distributor Using CSMP, a Simulation Language. *Transactions of the ASAE*, *17*(6), 1091–1093. https://doi.org/10.13031/2013.37036

J. P. Fulton, S. A. Shearer, S. F. Higgins, D. W. Hancock, & T. S. Stombaugh. (2005). Distribution Pattern Variability of Granular VRT Applicator. *Transactions of the ASAE*, *48*(6), 2053–2064. https://doi.org/10.13031/2013.20082

Jerry B. Davis & Charles E. Rice. (1973). Distribution of Granular Fertilizer and Wheat Seed by Centrifugal Distributors. *Transactions of the ASAE*, *16*(5), 0867–0868. https://doi.org/10.13031/2013.37646

John W. Glover & Jack V. Baird. (1973). Performance of Spinner Type Fertilizer Spreaders. *Transactions of the ASAE*, *16*(1), 0048–0051. https://doi.org/10.13031/2013.37441

Jonathan B Hall, John P Fulton, Timothy P McDonald, Wesley C Zech, Larry G Crowley, & Oladiran O Fasina. (2010). Using 3-D Simulation to Evaluate Spinner-disc Spreader Performance for Variable-Rate Application of Poultry Litter. *2010 Pittsburgh, Pennsylvania, June 20 - June 23, 2010*. 2010 Pittsburgh, Pennsylvania, June 20 - June 23, 2010. https://doi.org/10.13031/2013.36311

Kaye, J. P., & Quemada, M. (2017). Using cover crops to mitigate and adapt to climate change. A review. *Agronomy for Sustainable Development*, *37*(1), 4. https://doi.org/10.1007/s13593-016-0410-x

Kraus, T. (n.d.). *100 Years of Aerial Crop Dusting*. National Agricultural Aviation Association. Retrieved August 18, 2025, from https://www.faa.gov/sites/faa.gov/files/about/history/pioneers/100_Years_Aerial_Crop_Dusting.pdf

M. E. Teske, H. W. Thistle, & I. J. Grob. (2007). Determination of Dry Material Physical Characteristics for Use in Dispersion Modeling. *Transactions of the ASABE*, *50*(4), 1149–1156. https://doi.org/10.13031/2013.23624

Miclet, D., Piron, E., Beurrier, V., Crebassa, X., & Villette, S. (2011). *Slug pellet spreading: The double-disc performances available with a single disc spreader*.

National Transportation Safety Board. (2014). *Special Investigation Report on the Safety of Agricultural Aircraft Operations* (Nos. PB2014-105983). https://www.ntsb.gov/safety/safety-studies/documents/sir1401.pdf

Ozkan, E. (2024). *Drones for Spraying Pesticides—Opportunities and Challenges* (Extension Publication No. 540; Ohio State University. https://ohioline.osu.edu/factsheet/fabe-540

Przywara, A., Santoro, F., Kraszkiewicz, A., Pecyna, A., & Pascuzzi, S. (2020). Experimental Study of Disc Fertilizer Spreader Performance. *Agriculture*, *10*(10), 467. https://doi.org/10.3390/agriculture10100467

R. L. Parish. (1991). Effect of Material Bouncing Into and Out of Collection Pans on Observed Spreader Distribution Pattern. *Applied Engineering in Agriculture*, *7*(3), 311–315. https://doi.org/10.13031/2013.26239

R. W. Whitney, L. O. Roth, & D. K. Kuhlman. (1987). Performance of Selected Granular Collectors. *Transactions of the ASAE*, *30*(2), 0338–0342. https://doi.org/10.13031/2013.31950

Richard L. Parish & Patrick P. Chancy. (1986). Pattern Sensitivity to Location of Fertilizer Drop Point on a Rotary Spreader Impeller. *Transactions of the ASAE*, *29*(2), 0374–0377. https://doi.org/10.13031/2013.30156

Rorick, J. D., & Kladivko, E. J. (2017). Cereal rye cover crop effects on soil carbon and physical properties in southeastern Indiana. *Journal of Soil and Water Conservation*, *72*(3), 260–265. https://doi.org/10.2489/jswc.72.3.260

Roth, L. O., & Field, H. L. (1992). Machinery Calibration. In L. O. Roth & H. L. Field, *Introduction to Agricultural Engineering* (pp. 91–110). Springer US. https://doi.org/10.1007/978-1-4615-3594-2_9

Sarrantonio, M., & Gallandt, E. (2003). The Role of Cover Crops in North American Cropping Systems. *Journal of Crop Production*, *8*(1–2), 53–74. https://doi.org/10.1300/J144v08n01_04

Sever, M. (2023). Cereal Rye Among the Best Cover Crops at Weed Suppression. *Crops & Soils*, *56*(5), 58–62. https://doi.org/10.1002/crso.20308

Shaheb, M. R., Venkatesh, R., & Shearer, S. A. (2021). A Review on the Effect of Soil Compaction and its Management for Sustainable Crop Production. *Journal of Biosystems Engineering*, *46*(4), 417–439. https://doi.org/10.1007/s42853-021-00117-7

Sizemore, J., Virk, S., Gamble, A., Li, S., & Price, A. (2026). Application Rate Accuracy and Distribution Uniformity of Cover Crop Seeding with an Unmanned Aerial System (UAS). *Applied Engineering in Agriculture*, *42*(1), 93–103. https://doi.org/doi:%252010.13031/aea.16248

Song, C., Liu, L., Wang, G., Han, J., Zhang, T., & Lan, Y. (2023). Particle Deposition Distribution of Multi-Rotor UAV-Based Fertilizer Spreader under Different Height and Speed Parameters. *Drones*, *7*(7), 425. https://doi.org/10.3390/drones7070425

T. E. Grift. (2000). Spread Pattern Analysis Tool (Spat): I. Development and Theoretical Examples. *Transactions of the ASAE*, *43*(6), 1341–1350. https://doi.org/10.13031/2013.3031

Teske, M. E., Wachspress, D. A., & Thistle, H. W. (2018). Prediction of Aerial Spray Release from UAVs. *Transactions of the ASABE*, *61*(3), 909–918. https://doi.org/10.13031/trans.12701

Thomas, Jr., A. D. (2025). *Using Agricultural Drones for Spreading Granular Materials*. Ohio State University. https://etd.ohiolink.edu/acprod/odb_etd/etd/r/1501/10?clear=10&p10_accession_num=osu1744911938117787

Tony E. Grift & Giyoung Kweon. (2006). Development of a Uniformity Controlled Granular Fertilizer Spreader. 2006 Portland, Oregon, July 9-12, 2006. 2006 Portland, Oregon, July 9-12, 2006. https://doi.org/10.13031/2013.20594

United States Department of Agriculture. (2014). Conservation Practice Standard Overview. USDA. https://www.nrcs.usda.gov/sites/default/files/2022-09/Cover_Crop_340_Overview.pdf

United States Department of Agriculture. (2024, June 28). *USDA National Agriculture Statistics Service—Acreage Report 6/28/2024*. USDA. https://www.nass.usda.gov/Publications/Todays_Reports/reports/acrg0624.pdf

Vendig, I., Guzman, A., De La Cerda, G., Esquivel, K., Mayer, A. C., Ponisio, L., & Bowles, T. M. (2023). Quantifying direct yield benefits of soil carbon increases from cover cropping. *Nature Sustainability*, *6*(9), 1125–1134. https://doi.org/10.1038/s41893-023-01131-7

Wang, X., Jiang, R., Zhou, Z., Song, C., Luo, X., Bao, R., Lyu, Z., Huang, J., Lin, J. (2023). Discharge rate consistency of each channel for UAV-based pneumatic granular fertilizer spreader. *International Journal of Agricultural and Biological Engineering*, *16*(4), 20–28. https://doi.org/10.25165/j.ijabe.20231604.7129

Whalley, W. R., Dumitru, E., & Dexter, A. R. (1995). Biological effects of soil compaction. *Soil and Tillage Research*, *35*(1–2), 53–68. https://doi.org/10.1016/0167-1987(95)00473-6

Wilson, M. L., Allan, D. L., & Baker, J. M. (2014). Aerially seeding cover crops in the northern US Corn Belt: Limitations, future research needs, and alternative practices. *Journal of Soil and Water Conservation*, *69*(3), 1. https://doi.org/10.2489/jswc.69.3.67A

Wu, Z., Li, M., Lei, X., Wu, Z., Jiang, C., Zhou, L., Ma, R., & Chen, Y. (2020). Simulation and parameter optimisation of a centrifugal rice seeding spreader for a UAV. *Biosystems Engineering*, *192*, 275–293. https://doi.org/10.1016/j.biosystemseng.2020.02.004

Xia, X., Zhang, R., Ma, L., Su, J., Yi, T., Zhang, L., & Chen, X. (2025). Optimization of unmanned aerial vehicle operational parameters to maximize fertilizer application efficiency in rice cultivation. *Journal of Cleaner Production*, *514*, 145762. https://doi.org/10.1016/j.jclepro.2025.145762

Xiongkui, H., Bonds, J., Herbst, A., & Langenakens, J. (2017). Recent development of unmanned aerial vehicle for plant protection in East Asia. *International Journal of Agricultural and Biological Engineering*, *10*(3), 18–30. https://doi.org/10.3965/j.ijabe.20171003.3248

Xunwei, W., Zhiyan, Z., Boqian, C., Jinfeng, Z., Xiaolong, F., & Hewitt, A. (2024). Distribution uniformity improvement methods of a large discharge rate disc spreader for UAV fertilizer application. *Computers and Electronics in Agriculture*, *220*, 108928. https://doi.org/10.1016/j.compag.2024.108928

Y. Yildirim. (2008). Technical Note: Effect of Vane Shape on Fertilizer Distribution Uniformity in Single-Disc Rotary Fertilizer Spreaders. *Applied Engineering in Agriculture*, *24*(2), 159–163. https://doi.org/10.13031/2013.24261

Yallappa, D., Kavitha, R., Surendrakumar, A., Suthakar, B., Mohan Kumar, A. P., Kannan, B., & Kalarani, M. K. (2024). Improving agricultural spraying with multi-rotor drones: A technical study on operational parameter optimization. *Frontiers in Nutrition*, *11*, 1487074. https://doi.org/10.3389/fnut.2024.1487074

Yıldıran; Kara, Y. (2012). Effect of different vane combinations on fertilizer distribution uniformity with various flow rates in spinning disc broadcasters. *Tarım Bilimleri Dergisi*, *18*(1), 54–62. https://doi.org/10.1501/Tarimbil_0000001192

Zhang, R., Hewitt, A. J., Chen, L., Li, L., & Tang, Q. (2023). Challenges and opportunities of unmanned aerial vehicles as a new tool for crop pest control. *Pest Management Science*, *79*(11), 4123–4131. https://doi.org/10.1002/ps.7683

Appendices

Appendix A: Supplemental Information for Chapter 3

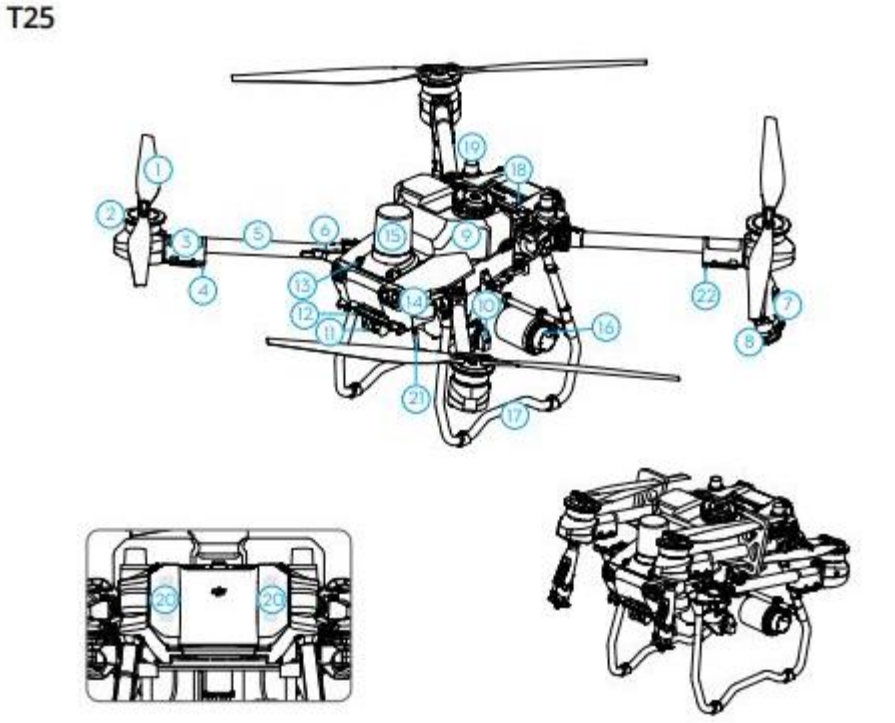

1. Propellers
2. Motors
3. ESCs
4. Aircraft Front Indicators (on two front arms)
5. Frame Arms
6. Folding Detection Sensors (built-in)
7. Spray Lance
8. Sprinklers
9. Spray Tank
10. Delivery Pumps
11. FPV Camera
12. Downward Binocular Vision
13. Forward Binocular Vision
14. Spotlights
15. Forward Phased Array Radar
16. Rear Phased Array Radar
17. Landing Gear
18. Intelligent Flight Battery
19. Onboard D-RTK Antennas
20. Internal Ocusync Image Transmission Antennas
21. External OcuSync Image Transmission Antennas
22. Aircraft Status Indicators (on two rear arms)

Figure A.1. DJI Agras T25 Diagram and Different Components.

T25

Aircraft	
Model	3WWDZ-20B
Weight	25.4 kg (excl. battery) 32 kg (inc. battery)
Max Takeoff Weight[1]	Max takeoff weight for spraying: 52 kg (at sea level) Max takeoff weight for spreading: 58 kg (at sea level)
Max Diagonal Wheelbase	1925 mm
Dimensions	2585×2675×780 mm (arms and propellers unfolded) 1475×1540×780 mm (arms unfolded and propellers folded) 1050×690×820 mm (arms and propellers folded)
Hovering Accuracy Range (with strong GNSS signal)	D-RTK enabled: Horizontal: ±10 cm, Vertical: ±10 cm D-RTK disabled: Horizontal: ±60 cm, Vertical: ±30 cm (radar module enabled: ±10 cm)
Operating Frequency[2]	2.4000-2.4835 GHz, 5.725-5.850 GHz
Transmitter Power (EIRP)	2.4 GHz: <20 dBm (SRRC/CE/MIC), <33 dBm (FCC) 5.8 GHz: <33 dBm (SRRC/FCC), <14 dBm (CE)
RTK/GNSS Operating Frequency	RTK: GPS L1/L2, GLONASS F1/F2, BeiDou B1I/B2I/B3I, Galileo E1/E5b, QZSS L1/L2 GNSS: GPS L1, GLONASS F1, Galileo E1, BeiDou B1I, QZSS L1
Hovering Time[3]	No payload for spraying: 14.5 min (takeoff weight of 32 kg with a 15.5Ah battery) Fully loaded for spraying: 7 min (takeoff weight of 52 kg with a 15.5Ah battery) No payload for spreading: 14.5 min (takeoff weight of 32 kg with a 15.5Ah battery) Fully loaded for spreading: 6 min (takeoff weight of 58 kg with a 15.5Ah battery)
Max Configurable Flight Radius	2000 m
Max Wind Resistance	6 m/s
Operating Temperature	0° to 45° C (32° to 113° F)

© 2024 DJI All Rights Reserved.

Figure A.2. DJI Agras T25 Specifications (1/4)

Propulsion System	
Motors	
Stator Size	100×28 mm
KV	59 rpm/V
Power	4600 W/rotor
Propellers	
Diameter	50 in (1270 mm)
Rotors Quantity	4
Dual Atomizing Spraying System	
Spray Tank	
Volume	20 L
Operating Payload[3]	20 kg
Sprinklers	
Model	LX8060SZ
Quantity	2
Droplet Size	50-500 μm
Max Effective Spray Width[4]	4-7 m (at a height of 3 m above the crops)
Delivery Pumps	
Type	Magnetic drive impeller pump
Max Flow Rate	16 L/min (2 sprinklers)
Phased Array Radar System	
Model	RD241608RF (forward phased array radar) RD241608RB (rear phased array radar)
Terrain Follow	Max slope in Mountain mode: 50° Altitude detection range: 1-50 m Stabilization working range: 1.5-30 m
Obstacle Avoidance[5]	Obstacle sensing range (omnidirectional): 1-50 m FOV: Forward phased array radar: horizontal 360°, vertical ±45°, upward ±45° (cone) Rear phased array radar: vertical 360°, horizontal ±45° Working conditions: flying higher than 1.5 m over the obstacle at a horizontal speed no more than 10 m/s and vertical speed no more than 3 m/s. Safety limit distance: 2.5 m (distance between the front of propellers and the obstacle after braking) Sensing direction: multidirectional obstacle sensing
Operating Frequency	24.05-24.25 GHz (NCC/FCC/MIC/KCC/CE)
Power Consumption	23 W (forward phased array radar) 18 W (rear phased array radar)
Transmitter Power (EIRP)	<20 dBm (NCC/FCC/MIC/KCC/CE)
Operating Voltage	DC 15V

 © 2024 DJI All Rights Reserved.

Figure A.3. DJI Agras T25 Specifications (2/4)

Operating Temperature	0° to 45° C (32° to 113° F)
Binocular Vision System	
Measurement Range	0.5-29 m
Effective Sensing Speed	≤10 m/s
FOV	Horizontal: 90°, Vertical: 106°
Operating Environment	Adequate light and discernible surroundings
Remote Controller	
Model	RM700B
GNSS	GPS + Galileo + BeiDou
Screen	7.02-in LCD touchscreen, with a resolution of 1920×1200 pixels, and high brightness of 1200 cd/m²
Operating Temperature	-20° to 50° C (-4° to 122° F)
Storage Temperature Range	Less than one month: -30° to 45° C (-22° to 113° F) One to three months: -30° to 35° C (-22° to 95° F) Three months to one year: -30° to 30° C (-22° to 86° F)
Charging Temperature	5° to 40° C (41° to 104° F)
Internal Battery Chemical System	LiNiCoAlO2
Internal Battery Runtime	3 hours 18 minutes
External Battery Runtime	2 hours 42 minutes
Charging Type	It is recommended to use a locally certified USB-C charger at a maximum rated power of 65 W and maximum voltage of 20 V such as the DJI 65W Portable Charger.
Charging Time	2 hours for internal battery or internal and external battery (when remote controller is powered off and using a standard DJI charger)
O3 Agras	
Operating Frequency[2]	2.4000-2.4835 GHz, 5.725-5.850 GHz
Transmitter Power (EIRP)	2.4 GHz: <33 dBm (FCC), <20 dBm (CE/SRRC/MIC) 5.8 GHz: <33 dBm (FCC), <14 dBm (CE), <23 dBm (SRRC)
Max Transmission Distance	7 km (FCC), 5 km (SRRC), 4 km (MIC/CE) (unobstructed, free of interference, and at an altitude of 2.5 m)
Wi-Fi	
Protocol	Wi-Fi 6
Operating Frequency[2]	2.4000-2.4835 GHz, 5.150-5.250 GHz, 5.725-5.850 GHz
Transmitter Power (EIRP)	2.4 GHz: <26 dBm (FCC), <20 dBm (CE/SRRC/MIC) 5.1 GHz: <26 dBm (FCC), <23 dBm (CE/SRRC/MIC) 5.8 GHz: <26 dBm (FCC/SRRC), <14 dBm (CE)
Bluetooth	
Protocol	Bluetooth 5.1
Operating Frequency	2.4000-2.4835 GHz
Transmitter Power (EIRP)	<10 dBm

© 2024 DJI All Rights Reserved.

Figure A.4. DJI Agras T25 Specifications (3/4)

[1] The DJI Agras app will intelligently recommend the payload weight limit for the tank according to the current status and surroundings of the aircraft. Do not exceed the recommended payload weight limit when adding material to the tank. Otherwise, the flight safety may be affected.

[2] 5.8 and 5.1 GHz frequencies are prohibited in some countries. In some countries, the 5.1 GHz frequency is only allowed for use indoors.

[3] Hovering time acquired at sea level with wind speed lower than 3 m/s and a temperature of 25° C (77° F). For reference only. The data may vary depending on the environment. Actual results shall be as tested.

[4] The spray width depends on the actual operation scenarios.

[5] The effective sensing range varies depending on the material, position, shape, and other properties of the obstacle. The downward sensing function is used to assist in Terrain Follow, while the sensing function on the other sides is for obstacle sensing.

Figure A.5. DJI Agras T25 Specifications (4/4)

Flow Calibration

There are several templates for typical spreading materials in the spreading settings of the DJI Agras app. Users can start spreading operations directly when using any of the templates. Users can also create templates if the performance of the templates in the app are not satisfactory or if other spreading materials are being used. Flow calibration is required when creating a new template. Refer to the Usage section for more information about creating templates.

- Calibration is required after replacing the hopper gate to ensure the operation accuracy.

Usage

Creating Templates

If the performance of the existing templates are unsatisfactory or other materials are being used, users can create a new template as follows:

1. Disassemble the spinner disk according to the instructions in the Maintenance section. Make sure to store the removed pin, nut, and washer carefully.
2. Place the aircraft on a flat surface. It is recommended to place a plastic sheet or film below the hopper outlet to collect the dispensed material. Add the used material into the spread tank and close the cover. It is recommended to add more than 15 kg of the material.
3. Make sure the spreading system cable is connected and then power on the remote controller and aircraft.
4. Go to Operation View in the app, tap ⚙, then 🏆, and tap Materials Management. Select Add New Material and then set the type of the hopper outlet in use.

   - When using the standard hopper gate that is pre-mounted on with the spreading system, make sure to set the hopper outlet type to Hopper Outlet 1. When using the small flow hopper gate that is sold separately, make sure to set the hopper outlet type to Hopper Outlet 2. Refer to the Replacing Hopper Gate section to learn how to replace the hopper gate and the recommended materials.

5. Tap Calibrate and the spreading system will start working during the calibration.
6. Set the material amount, spinner disk speed, and flight speed after calibration and tap Save.
7. Power off the aircraft and remount the spinner disk.

Figure A.6. DJI Agras T25 Calibration Instructions for Dry Materials

Specifications

Specifications	T50 Spreading System	T25 Spreading System
Compatible Aircraft[1]	Agras T50	Agras T25
Spreading System Weight (inc. spread tank and fenders)	6.0 kg	3.9 kg
Spread Tank Volume	75 L	35 L
Spread Tank Internal Load[2]	50 kg	25 kg
Compatible Material Diameter	0.5-5 mm	
Spreading Range	Varies according to the material diameter, spinner disk rotational speed, hopper outlet size, and flight altitude. For optimal performance, it is recommended to adjust the corresponding variables to achieve a spreading range of 4.5-7 meters.	

[1] The aircraft firmware must support the spreading system. Check the release notes of the corresponding aircraft on the official DJI website.

[2] The DJI Agras app will intelligently recommend the payload weight limit for the spread tank according to the current status and the surroundings of the aircraft. DO NOT exceed the recommended payload weight limit when adding the material to the spread tank. Otherwise, flight safety may be affected.

 © 2024 DJI All Rights Reserved.

Figure A.7. Specifications of the Dry Spreading System on DJI Agras T25.

Table A.1. Meteorological data for the field test involving different application rates.

Rate Test (kg ha^{-1})	Replication	Wind Speed (m s^{-1})	Direction	Temp (C°)	Humidity (%)
22.4	1	1.34	NW	10.6	76.0
22.4	2	1.34	NW	10.6	75.0
22.4	3	0.89	NNE	10.6	74.0
22.4	4	1.79	N	10.6	75.0
33.6	1	1.34	NNE	11.1	74.0
33.6	2	2.24	NNE	11.1	73.0
33.6	3	0.45	N	11.1	68.0
33.6	4	1.34	NE	11.1	73.0
44.8	1	0.89	N	11.7	72.0
44.8	2	1.34	NNE	11.7	70.0
44.8	3	0.89	N	11.1	71.0
44.8	4	0.89	NNW	11.7	72.0
56.0	1	2.24	ENE	11.7	71.0
56.0	2	2.24	ENE	11.7	70.0
56.0	3	0.89	N	11.7	69.0
56.0	4	0.45	NE	11.7	69.0
64.3	1	0.89	NW	11.7	70.0
64.3	2	1.79	NE	12.2	69.0
64.3	3	2.24	NW	12.8	68.0
64.3	4	2.24	NE	12.8	69.0

Table A.2. Meteorological data for the field test involving different flight speeds.

Rate Test (kg ha^{-1})	Replication	Wind Speed (m s^{-1})	Direction	Temp (C°)	Humidity (%)
6.0	1	1.34	WNW	15.0	58.0
6.0	2	1.79	WNW	15.0	59.0
6.0	3	1.79	WNW	15.0	59.0
6.0	4	1.79	WNW	15.0	60.0
7.0	1	0.89	WSW	13.9	64.0
7.0	2	1.34	W	13.9	64.0
7.0	3	1.79	W	13.9	65.0
7.0	4	0.89	W	13.9	64.0
8.0	1	1.79	W	14.4	62.0
8.0	2	1.34	W	14.4	61.0
8.0	3	0.89	W	14.4	62.0
8.0	4	1.34	WNW	14.4	62.0
9.0	1	1.79	W	14.4	62.0
9.0	2	1.34	W	14.4	62.0
9.0	3	0.89	W	14.4	63.0
9.0	4	1.79	W	14.4	62.0
10.0	1	0.89	WNW	12.8	66.0
10.0	2	0.89	W	12.8	67.0
10.0	3	0.89	WNW	12.2	67.0
10.0	4	0.45	WNW	12.2	68.0

Appendix B: Supplemental Information for Chapter 4

Table B.1. Meteorological data for the spinner disc rpm and flight height field tests.

Spinner Disc Speed (RPM)	Flight Height (m)	Replication	Wind Speed (m s^{-1})	Direction	Temp (C°)	Humidity (%)
700	3.0	1	0.89	SE	30.6	47.0
700	3.0	2	0.89	E	30.6	48.0
700	3.0	3	0.89	NE	30.6	49.0
700	3.0	4	1.34	NW	30.6	49.0
1000	3.0	1	1.34	NNE	30.6	50.0
1000	3.0	2	0.89	N	30.6	48.0
1000	3.0	3	0.45	N	30.6	49.0
1000	3.0	4	1.34	N	30.6	49.0
1300	3.0	1	1.34	N	30.6	50.0
1300	3.0	2	0.45	NE	30.6	48.0
1300	3.0	3	1.34	SE	30.6	48.0
1300	3.0	4	0.89	SE	30.6	48.0
700	3.8	1	0.45	NE	30.6	50.0
700	3.8	2	0.45	ESE	30.6	49.0
700	3.8	3	1.34	ENE	30.6	50.0
700	3.8	4	2.24	NNE	30.6	49.0
1000	3.8	1	0.89	N	30.0	51.0
1000	3.8	2	0.89	SE	30.0	48.0
1000	3.8	3	0.89	NNE	30.0	51.0
1000	3.8	4	0.00	-	30.6	49.0
1300	3.8	1	2.24	NNW	30.6	53.0
1300	3.8	2	1.34	N	30.6	50.0
1300	3.8	3	1.34	ESE	30.0	50.0
1300	3.8	4	0.45	SE	30.0	50.0
700	4.6	1	0.89	N	30.6	50.0
700	4.6	2	0.89	N	30.6	51.0
700	4.6	3	0.45	ENE	30.6	51.0
700	4.6	4	0.89	NE	30.6	50.0
1000	4.6	1	2.68	NNW	29.4	54.0
1000	4.6	2	0.00	-	30.0	52.0
1000	4.6	3	2.24	ENE	30.0	52.0
1000	4.6	4	1.34	NW	30.0	52.0
1300	4.6	1	0.45	S	28.3	57.0
1300	4.6	2	0.45	S	28.9	55.0
1300	4.6	3	1.34	NNW	28.3	58.0
1300	4.6	4	0.89	SW	28.9	56.0

Table B.2. Meteorological data for the gate design and application rate field test.

Gate Design	Application Rate (kg ha^{-1})	Replication	Wind Speed (m s^{-1})	Direction	Temp (C°)	Humidity (%)
Large	22.4	1	0.00	-	20.0	85.0
Large	22.4	2	0.00	-	20.0	85.0
Large	22.4	3	0.00	-	20.0	86.0
Large	22.4	4	0.00	-	20.0	86.0
Large	33.6	1	0.00	-	20.6	86.0
Large	33.6	2	0.45	W	20.0	85.0
Large	33.6	3	0.00	-	21.1	85.0
Large	33.6	4	1.34	E	21.7	84.0
Large	44.8	1	0.89	SSE	22.2	83.0
Large	44.8	2	0.89	SSE	22.2	83.0
Large	44.8	3	1.34	SSE	22.8	80.0
Large	44.8	4	1.34	SSW	22.8	80.0
Medium	22.4	1	0.45	ESE	23.9	77.0
Medium	22.4	2	0.45	S	24.4	75.0
Medium	22.4	3	2.24	S	24.4	74.0
Medium	22.4	4	2.68	SSE	25.0	73.0
Medium	33.6	1	2.68	S	25.0	73.0
Medium	33.6	2	1.34	SSE	25.0	71.0
Medium	33.6	3	1.79	ESE	25.6	70.0
Medium	33.6	4		S	25.6	68.0
Medium	44.8	1	2.24	ENE	25.6	69.0
Medium	44.8	2	2.24	S	26.1	70.0
Medium	44.8	3	1.79	SSW	26.1	66.0
Medium	44.8	4	1.79	S	26.1	66.0

Table B.3. Meteorological data spreading disc design and application rate field test.

Disc Design	Application Rate (kg ha^{-1})	Replication	Wind Speed (m s^{-1})	Direction	Temp (C°)	Humidity (%)
Curved	33.6	1	1.34	NNE	22.8	78.0
Curved	33.6	2	0.45	ESE	22.8	78.0
Curved	33.6	3	0.89	ESE	23.3	78.0
Curved	33.6	4	0.00	-	23.3	76.0
Curved	44.8	1	1.34	NNE	23.3	76.0
Curved	44.8	2	0.00	-	23.3	77.0
Curved	44.8	3	0.89	E	23.3	77.0
Curved	44.8	4	0.89	N	23.3	75.0
Curved	56.0	1	0.45	WNW	23.9	75.0
Curved	56.0	2	0.00	-	23.9	75.0
Curved	56.0	3	0.45	NNE	23.9	76.0
Curved	56.0	4	0.00	-	23.9	75.0
Straight	33.6	1	0.00	-	23.9	75.0
Straight	33.6	2	0.00	-	24.4	73.0
Straight	33.6	3	0.89	NNE	24.4	74.0
Straight	33.6	4	0.45	ENE	24.4	74.0
Straight	44.8	1	0.00	-	24.4	73.0
Straight	44.8	2	0.45	ENE	24.4	73.0
Straight	44.8	3	0.00	-	25.0	74.0
Straight	44.8	4	0.00	NNE	25.6	72.0
Straight	56.0	1	1.34	NE	25.6	71.0
Straight	56.0	2	0.45	WSW	25.6	71.0
Straight	56.0	3	0.89	SE	26.1	71.0
Straight	56.0	4	0.45	W	26.7	69.0

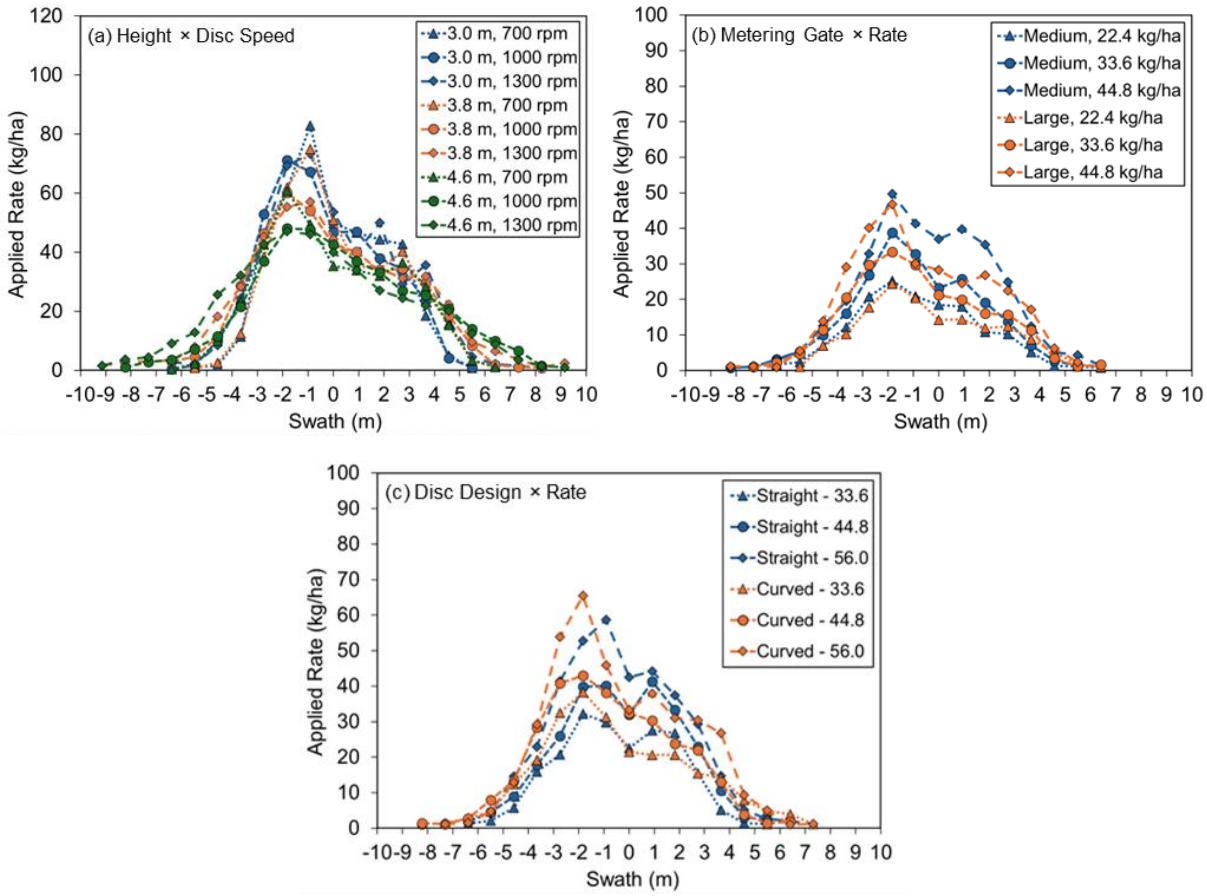

Figure B.1. Single-pass distribution patterns for cereal rye applied with a UAS at different (a) application heights and spinner-disc speeds, and (b) metering gates, and (c) spreading discs (different vane designs) tested across different application rates. 0 m on the graph coincides with the center of the UAS flight path.

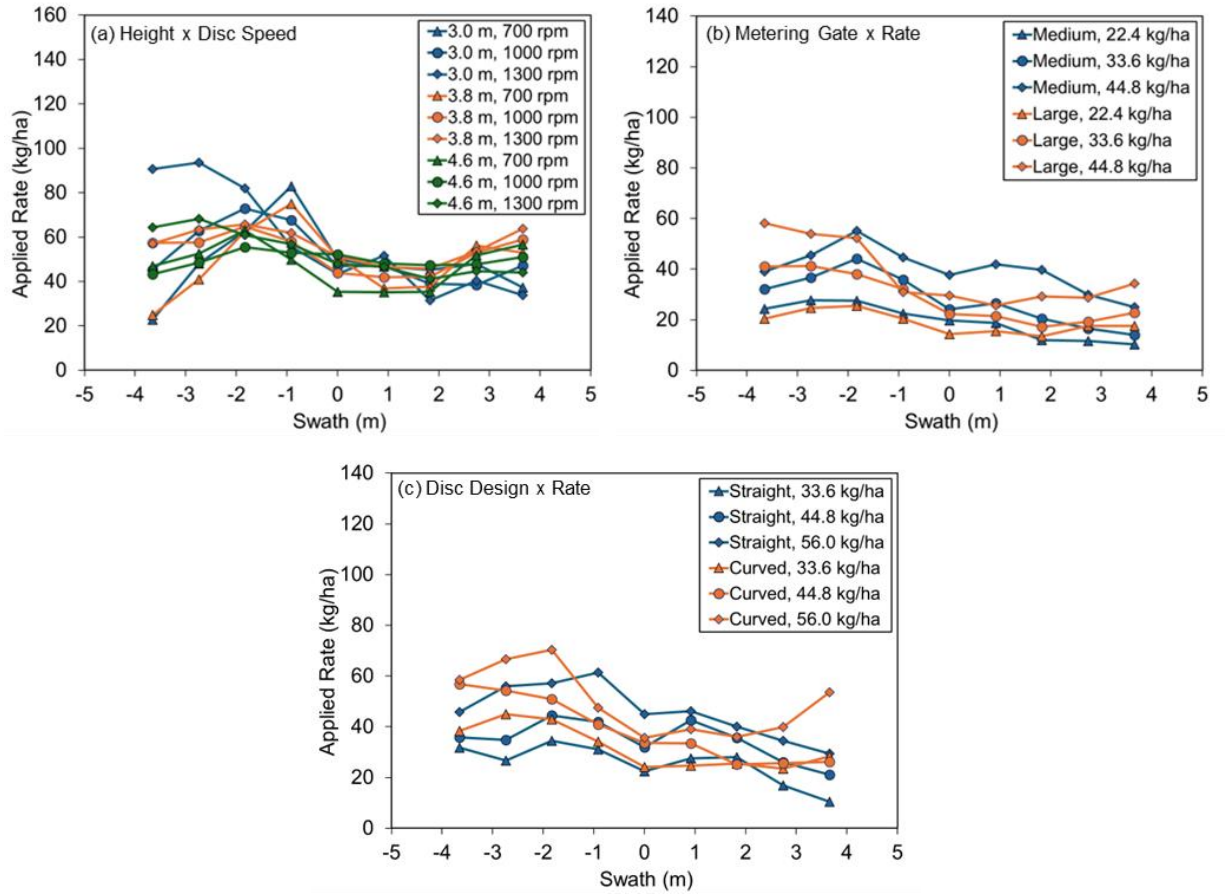

Figure B.2. Simulated overlap spread patterns using progressive application method for cereal rye applied with a UAS at different (a) application heights and spinner-disc speeds, and (b) metering gates, and (c) spreading discs (vane designs) tested across different application rates. 0 m on the graph coincides with the center of the UAS flight path.

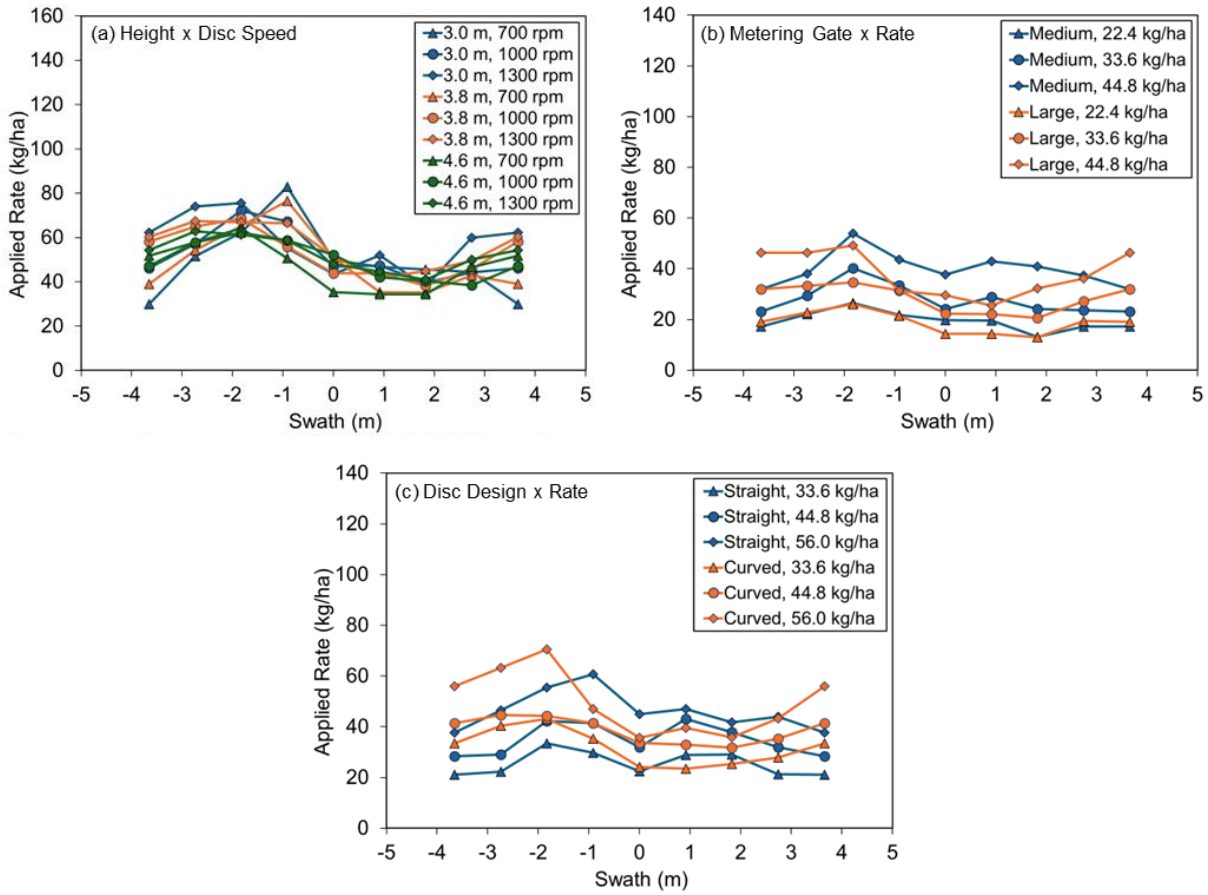

Figure B.3. Simulated overlap spread patterns using one-direction application method for cereal rye applied with a UAS at different (a) application heights and spinner-disc speeds, and (b) metering gates, and (c) spreading discs (vane designs) tested across different application rates. 0 m on the graph coincides with the center of the UAS flight path.